



PUBLISHED FOR SISSA BY SPRINGER

RECEIVED: November 23, 2010

REVISED: February 2, 2011

ACCEPTED: February 25, 2011

PUBLISHED: March 11, 2011

Neutrino mass hierarchy determination using reactor antineutrinos

Pomita Ghoshal^a and S.T. Petcov^{a,b,1}

^aSISSA and INFN-Sezione di Trieste,
via Bonomea 265, 34136 Trieste, Italy

^bIPMU, University of Tokyo,
Tokyo, Japan

E-mail: pghoshal@sissa.it, petcov@sissa.it

ABSTRACT: Building on earlier studies, we investigate the possibility to determine the type of neutrino mass spectrum (i.e., “the neutrino mass hierarchy”) in a high statistics reactor $\bar{\nu}_e$ experiment with a relatively large KamLAND-like detector and an optimal baseline of 60 Km. We analyze systematically the Fourier Sine and Cosine Transforms (FST and FCT) of simulated reactor antineutrino data with reference to their specific mass hierarchy-dependent features discussed earlier in the literature. We perform also a binned χ^2 analysis of the sensitivity of simulated reactor $\bar{\nu}_e$ event spectrum data to the neutrino mass hierarchy, and determine, in particular, the characteristics of the detector and the experiment (energy resolution, visible energy threshold, exposure, systematic errors, binning of data, etc.), which would allow us to get significant information on, or even determine, the type of the neutrino mass spectrum. We find that if $\sin^2 2\theta_{13}$ is sufficiently large, $\sin^2 2\theta_{13} \gtrsim 0.02$, the requirements on the set-up of interest are very challenging, but not impossible to realize.

KEYWORDS: Neutrino Physics, Beyond Standard Model

ARXIV EPRINT: [1011.1646](https://arxiv.org/abs/1011.1646)

¹Also at: Institute of Nuclear Research and Nuclear Energy, Bulgarian Academy of Sciences, 1784 Sofia, Bulgaria.

Contents

1	Introduction	1
2	Preliminary remarks	5
3	The effects of energy smearing and energy scale uncertainty on the reactor $\bar{\nu}_e$ event rate and Fourier spectra	8
3.1	Behaviour of the event rate spectrum	8
3.2	Fourier analysis of the reactor $\bar{\nu}_e$ event rate spectrum	10
3.3	The effect of the uncertainty of Δm_{31}^2 on the Fourier spectra	17
4	χ^2-analysis of the sensitivity to the type of the neutrino mass spectrum	17
4.1	Parameter marginalization	19
4.2	The precision on Δm_{atm}^2 and its effect on the hierarchy sensitivity	21
4.3	Results	23
5	Conclusions	26

1 Introduction

The experiments with solar, atmospheric, reactor and accelerator neutrinos [1–18] have provided compelling evidences for the existence of flavour neutrino oscillations [19–21] caused by nonzero neutrino masses and neutrino mixing. The data imply the presence of neutrino mixing in the weak charged lepton current:

$$\nu_{lL}(x) = \sum_j U_{lj} \nu_{jL}(x), \quad l = e, \mu, \tau, \quad (1.1)$$

where ν_{lL} are the flavour neutrino fields, $\nu_{jL}(x)$ is the left-handed (LH) component of the field of the neutrino ν_j possessing a mass m_j and U is a unitary matrix - the Pontecorvo-Maki-Nakagawa-Sakata (PMNS) neutrino mixing matrix [19–22].

All compelling neutrino oscillation data can be described assuming 3-flavour neutrino mixing in vacuum. The data on the invisible decay width of the Z^0 -boson is compatible with only 3 light flavour neutrinos coupled to Z^0 (see, e.g. [23]). The number of massive neutrinos ν_j , n , can, in general, be greater than 3, $n > 3$, if, for instance, there exist right-handed (RH) sterile neutrinos [22] and they mix with the LH flavour neutrinos. It follows from the existing data that at least 3 of the neutrinos ν_j , say ν_1, ν_2, ν_3 , must be light, $m_{1,2,3} \lesssim 1 \text{ eV}$, and must have different masses, $m_1 \neq m_2 \neq m_3$. At present there are no compelling experimental evidences for the existence of more than 3 light neutrinos.

Being electrically neutral, the massive neutrinos ν_j can be Dirac fermions (possessing distinctive antiparticles), or Majorana particles (which are identical with their respective

antiparticles, see, e.g., [24]). On the basis of the existing neutrino data it is impossible to determine whether the massive neutrinos are Dirac or Majorana fermions.

In the case of 3 light neutrinos, the neutrino mixing matrix U can be parametrized by 3 angles and, depending on whether the massive neutrinos ν_j are Dirac or Majorana particles, by 1 or 3 CP violation (CPV) phases [25]:

$$U_{\text{PMNS}} = \begin{pmatrix} c_{12}c_{13} & s_{12}c_{13} & s_{13}e^{-i\delta} \\ -s_{12}c_{23} - c_{12}s_{23}s_{13}e^{i\delta} & c_{12}c_{23} - s_{12}s_{23}s_{13}e^{i\delta} & s_{23}c_{13} \\ s_{12}s_{23} - c_{12}c_{23}s_{13}e^{i\delta} & -c_{12}s_{23} - s_{12}c_{23}s_{13}e^{i\delta} & c_{23}c_{13} \end{pmatrix} \text{diag}(1, e^{i\frac{\alpha_{21}}{2}}, e^{i\frac{\alpha_{31}}{2}}) \quad (1.2)$$

where $c_{ij} \equiv \cos \theta_{ij}$, $s_{ij} \equiv \sin \theta_{ij}$, $\theta_{ij} = [0, \pi/2]$, $\delta = [0, 2\pi]$ is the Dirac CP-violation (CPV) phase and α_{21}, α_{31} are two Majorana CPV phases.¹ If one identifies $\Delta m_{21}^2 > 0$ and Δm_{31}^2 (or Δm_{32}^2) with the neutrino mass squared differences which drive the solar and atmospheric neutrino oscillations, θ_{12} and θ_{23} represent the solar and atmospheric neutrino mixing angles, while θ_{13} is the CHOOZ angle [38]. The existing oscillation data allow us to determine $\Delta m_{21}^2 \equiv \Delta m_{\odot}^2$, θ_{12} , and $|\Delta m_{31}^2| \equiv |\Delta m_{\text{atm}}^2|$, θ_{23} , with a relatively good precision [39–41], and to obtain rather stringent limits on the angle θ_{13} [38]. The best fit values and the 99.73% C.L. allowed ranges of Δm_{21}^2 , $\sin^2 \theta_{12}$, $|\Delta m_{31(32)}^2|$ and $\sin^2 \theta_{23}$, read [41]:

$$\Delta m_{21}^2 = 7.59_{-0.18}^{+0.23} \times 10^{-5} \text{ eV}^2, \quad \Delta m_{21}^2 = (7.03 - 8.27) \times 10^{-5} \text{ eV}^2, \quad (1.3)$$

$$\sin^2 \theta_{12} = 0.318_{-0.016}^{+0.019}, \quad 0.27 \leq \sin^2 \theta_{12} \leq 0.38, \quad (1.4)$$

$$|\Delta m_{31}^2| = 2.40_{-0.11}^{+0.12} \times 10^{-3} \text{ eV}^2, \quad |\Delta m_{31}^2| = (2.07 - 2.75) \times 10^{-3} \text{ eV}^2, \quad (1.5)$$

$$\sin^2 \theta_{23} = 0.5_{-0.06}^{+0.07}, \quad 0.36 \leq \sin^2 \theta_{23} \leq 0.67. \quad (1.6)$$

Thus, we have $|\Delta m_{31(32)}^2| \gg \Delta m_{21}^2$, $\Delta m_{21}^2/|\Delta m_{31}^2| \cong 0.03$, and $|\Delta m_{31}^2| = |\Delta m_{32}^2 - \Delta m_{21}^2| \cong |\Delta m_{32}^2|$. Maximal solar neutrino mixing, i.e. $\theta_{12} = \pi/4$, is ruled out at more than 6σ by the data. Correspondingly, one has $\cos 2\theta_{12} \geq 0.26$ (at 99.73% C.L.). A combined 3-neutrino oscillation analysis of the global data gives [42]:

$$\sin^2 \theta_{13} < 0.031 \text{ (0.047)} \quad \text{at 90\% (99.73\%) C.L.} \quad (1.7)$$

The results of the global analyzes include also a weak indication of nonzero $\sin^2 \theta_{13} \sim 0.01$ (for a review see [42]). If $\theta_{13} \neq 0$, the Dirac phase δ can generate CP violation effects in neutrino oscillations [25, 43, 44]. The size of the indicated leptonic CP violation effects depends on the magnitude of the currently unknown values of θ_{13} and δ [45].

¹The two Majorana CP-violation phases [25] do not enter into the expressions for the oscillation probabilities of interest [25, 26] and we are not going to discuss them further. They play important role in the phenomenology of neutrinoless double beta decay (see, e.g., [27–29]). The phases $\alpha_{21,31}$ can affect significantly the predictions for the rates of the (LFV) decays $\mu \rightarrow e + \gamma$, $\tau \rightarrow \mu + \gamma$, etc. in a large class of supersymmetric theories incorporating the see-saw mechanism [30–32]. The Majorana phases can provide the CP violation, necessary for the generation of the baryon asymmetry of the Universe in the leptogenesis scenario of the asymmetry origins. [33–37].

The existing data do not allow us to determine the sign of $\Delta m_{31(32)}^2$. The two possibilities, $\Delta m_{31(32)}^2 > 0$ or $\Delta m_{31(32)}^2 < 0$, as is well known, correspond to two different types of neutrino mass spectrum: with normal ordering (hierarchy (NO,NH)), $m_1 < m_2 < m_3$, and with inverted ordering (hierarchy (IO,IH)), $m_3 < m_1 < m_2$.

Determining the nature - Dirac or Majorana, of massive neutrinos, getting more precise information about the value of the mixing angle θ_{13} , determining the sign of Δm_{31}^2 , or the type of the neutrino mass spectrum (with normal or inverted ordering (hierarchy)²) and getting information about the status of the CP symmetry in the lepton sector are among the major and remarkably challenging goals of future studies in neutrino physics (see, e.g., [42, 46, 47]). Establishing whether the neutrino mass spectrum is with normal or inverted hierarchy, i.e., measuring the sign of Δm_{31}^2 and determining the nature of massive neutrinos, in particular, are of fundamental importance for understanding the origin of neutrino masses and mixing (see, e.g., [48]).

In the present article we continue the studies of the possibility to obtain information about the type of spectrum the light neutrino masses obey (i.e., about $\text{sgn}(\Delta m_{31}^2)$) in experiments with reactor antineutrinos. This possibility was discussed first in [49] and later was further investigated in [50–54]. It is based on the observation that for $\cos 2\theta_{12} \neq 0$ and $\sin \theta_{13} \neq 0$, the probabilities of $\bar{\nu}_e$ survival in the cases of NO (NH) and IO (IH) spectra differ [49, 55]: $P^{\text{NH}}(\bar{\nu}_e \rightarrow \bar{\nu}_e) \neq P^{\text{IH}}(\bar{\nu}_e \rightarrow \bar{\nu}_e)$. For sufficiently large $|\cos 2\theta_{12}|$ and $\sin^2 \theta_{13}$ and a baseline of several tens of kilometers, this difference in the $\bar{\nu}_e$ oscillations leads, in principle, to an observable difference in the deformations of the spectrum of e^+ [49], produced in the inverse beta-decay reaction $\bar{\nu}_e + p \rightarrow e^+ + n$ by which the reactor $\bar{\nu}_e$ are detected. In [50] the physics potential of a reactor neutrino experiment with a relatively large detector at a distance of several tens of kilometers has been analyzed in detail. More specifically, the strategies and the experimental set-up, which would permit to measure Δm_{21}^2 and $\sin^2 \theta_{12}$ with a high precision, get information on (or even measure) $\sin^2 \theta_{13}$, and if $\sin^2 \theta_{13}$ is sufficiently large ($\sin^2 \theta_{13} \gtrsim 0.02$) provide a high precision measurement of Δm_{atm}^2 and determine the type of the neutrino mass hierarchy, have been discussed. The impact that i) the choice of the baseline L , ii) the effect of using a relatively low e^+ –energy cut-off of $E_{th} \sim 1.0 \text{ MeV}$, iii) the detector’s energy resolution, as well as iv) the statistical and systematical errors, can have on the measurement of each of the indicated neutrino oscillation parameters and on the determination of the neutrino mass hierarchy have also been investigated in [50].

In [51] a Fourier analysis of reactor $\bar{\nu}_e$ simulated data using the exponential Fourier transform (FT) was performed. It was found that the NH and IH neutrino mass spectra are distinguished by a relatively small shoulder beside the Δm_{atm}^2 modulation peak, which for the NH (IH) spectrum is to the left (to the right) of the peak. In the same study results of a statistical analysis of the possibility to determine the neutrino mass hierarchy for different baselines, different values of θ_{13} and different detector exposures (statistics) were also

²We use here and in what follows the generic terms “normal hierarchical” and “inverted hierarchical” for the neutrino mass spectra with normal ordering and inverted ordering, i.e., the spectra need not necessarily be hierarchical. We will use also the widely accepted term “neutrino mass hierarchy” for $\text{sgn}(\Delta m_{\text{atm}}^2)$ (i.e., for the neutrino mass ordering).

presented. In that analysis the effects of the detector energy resolution were accounted for, but the systematic uncertainties and the uncertainties in the energy scale and the neutrino oscillation parameters were not taken into account. The latter were included in an unbinned maximum likelihood analysis performed in [52].

It was noticed in [53, 54] that the sine and cosine Fourier transforms of simulated reactor $\bar{\nu}_e$ data in the case of NH and IH spectrum show a difference in certain specific features which can be used to distinguish between the two types of spectrum. The authors of [53, 54] include in their numerical simulations the effects of the detector's energy resolution and an uncertainty in the energy scale (shift and shrink/expansion), which is independent of energy. They do a statistical hierarchy analysis similar to that performed in [51] and give results for different values of θ_{13} , of the energy resolution and exposures. No systematic uncertainties or parameter marginalization were taken into account in this investigation. The possibility of an energy-dependent energy scale uncertainty was not considered either.

The present article is a natural continuation of the studies performed in [49–54]. More specifically, we investigate further the behaviour of the sine and cosine Fourier transformed e^+ spectra taking into account, in particular, the possibility of an energy-dependent energy scale uncertainty (assuming the shrink/expansion factor to have a linear dependence on the neutrino energy). In general, the mass hierarchy-dependent features of the Fourier spectra of interest are changed in the case of an energy-dependent energy scale shift. This might affect a statistical analysis using the FT method. We perform also a χ^2 analysis of the sensitivity to the neutrino mass hierarchy using simulated reactor $\bar{\nu}_e$ data. In this analysis we take into account a marginalization over the relevant neutrino oscillation parameters, the detector resolution, the energy scale uncertainty (both energy-dependent and independent) and the systematic errors. A χ^2 analysis offers the advantage of a binned study in which the binning (the division of the L/E range into bins) is optimized on the basis of the energy resolution and the improvement in sensitivity so as to give the best possible sensitivity to the neutrino mass hierarchy while being consistent with the detector's energy resolution. The systematic uncertainties are included using the method of pulls. We present results, in particular, for different values of the detector's energy resolution, exposure and θ_{13} .

Let us note that the type of neutrino mass hierarchy, i.e. $\text{sgn}(\Delta m_{31}^2)$, can be determined by studying oscillations of neutrinos and antineutrinos, say, $\nu_\mu \leftrightarrow \nu_e$ and $\bar{\nu}_\mu \leftrightarrow \bar{\nu}_e$, in which matter effects are sufficiently large. This can be done in long base-line ν -oscillation experiments (see, e.g. [47, 56–58]). If $\sin^2 2\theta_{13} \gtrsim 0.05$ and $\sin^2 \theta_{23} \gtrsim 0.50$, information on $\text{sgn}(\Delta m_{31}^2)$ might be obtained in atmospheric neutrino experiments by investigating the matter effects in the subdominant transitions $\nu_{\mu(e)} \rightarrow \nu_{e(\mu)}$ and $\bar{\nu}_{\mu(e)} \rightarrow \bar{\nu}_{e(\mu)}$ of atmospheric neutrinos which traverse the Earth [59–62], or by studying the “disappearance” of the atmospheric ν_μ and $\bar{\nu}_\mu$ crossing the Earth [62–64]. For $\nu_{\mu(e)}$ (or $\bar{\nu}_{\mu(e)}$) crossing the Earth core, a new type of resonance-like enhancement of the indicated transitions takes place due to the (*Earth*) *mantle-core constructive interference effect (neutrino oscillation length resonance (NOLR))* [65].³ For $\Delta m_{31}^2 > 0$, the neutrino transitions $\nu_{\mu(e)} \rightarrow \nu_{e(\mu)}$ are enhanced,

³As a consequence of this effect the indicated $\nu_{\mu(e)}$ (or $\bar{\nu}_{\mu(e)}$) transition probabilities can be maximal [66–68] (for the precise conditions of the mantle-core (NOLR) enhancement see [65–68]). Let us note that the

while for $\Delta m_{31}^2 < 0$ the enhancement of antineutrino transitions $\bar{\nu}_{\mu(e)} \rightarrow \bar{\nu}_{e(\mu)}$ takes place, which might allow to determine $\text{sgn}(\Delta m_{31}^2)$. If neutrinos with definite mass are Majorana particles, information about the $\text{sgn}(\Delta m_{31}^2)$ could be obtained also by measuring the effective neutrino Majorana mass in neutrinoless double β -decay experiments [27–29, 69, 70]. Information on the type of neutrino mass spectrum can also be obtained in β -decay experiments having a sensitivity to neutrino masses $\sim \sqrt{|\Delta m_{31}^2|} \cong 5 \times 10^{-2}$ eV [71] (i.e. by a factor of ~ 4 better sensitivity than that of the KATRIN experiment [72]).

2 Preliminary remarks

We consider an experimental set-up with a nuclear reactor producing electron antineutrinos by the β -decay of fission products of the isotopes U-235, U-238, Pu-239 and Pu-241. The $\bar{\nu}_e$ are assumed to be detected in a single KamLAND-like [12, 13] liquid scintillator detector, located at a distance of 60 Km from the reactor, by the inverse β -decay reaction:

$$\bar{\nu}_e + p \rightarrow e^+ + n. \tag{2.1}$$

The visible energy of the detected positron is given by

$$E_{\text{vis}} = E + m_e - (m_n - m_p) \tag{2.2}$$

$$\simeq E - 0.8 \text{ MeV} \tag{2.3}$$

Here m_e, m_n and m_p are the masses of the positron, neutron and proton, respectively, and E is the $\bar{\nu}_e$ energy. The no-oscillation event rate spectrum is the product of the initial $\bar{\nu}_e$ flux spectrum and the inverse β -decay cross-section and is bell-shaped, with its peak at about $E_{\text{vis}} = 2.8$ MeV. In the present analysis we use the analytic expression for the $\bar{\nu}_e$ flux spectrum given in [73]. The latter has a fit error of about 1.2% on the total event rate. The expression for the $\bar{\nu}_e + p \rightarrow e^+ + n$ cross-section is taken from [74]. The threshold of the visible energy used is $E_{\text{visth}} = 1.0$ MeV (see further).

The event rate spectrum is given by the product of the no-oscillation spectrum and the $\bar{\nu}_e$ survival probability $P_{\bar{e}\bar{e}}$. In the convention we are using the expression for the $\bar{\nu}_e$ survival probability in the case of 3 flavor neutrino mixing and NH(IH) neutrino mass spectrum is given by⁴ [49, 55]:

$$\begin{aligned} P_{\text{NH(IH)}}(\bar{\nu}_e \rightarrow \bar{\nu}_e) &\equiv P_{\bar{e}\bar{e}}^{\text{NH(IH)}} \\ &= 1 - 2 \sin^2 \theta_{13} \cos^2 \theta_{13} \left(1 - \cos \frac{\Delta m_{\text{atm}}^2 L}{2E} \right) \\ &\quad - \frac{1}{2} \cos^4 \theta_{13} \sin^2 2\theta_{12} \left(1 - \cos \frac{\Delta m_{\odot}^2 L}{2E} \right) \\ &\quad + 2a_{\text{NH(IH)}}^2 \sin^2 \theta_{13} \cos^2 \theta_{13} \left(\cos \left(\frac{\Delta m_{\text{atm}}^2 L}{2E} - \frac{\Delta m_{\odot}^2 L}{2E} \right) - \cos \frac{\Delta m_{\text{atm}}^2 L}{2E} \right), \end{aligned} \tag{2.4}$$

Earth mantle-core (NOLR) enhancement of neutrino transitions differs [65] from the MSW one.

⁴The Earth matter effects are negligible for the values of the neutrino oscillation parameters (Δm_{21}^2 and Δm_{31}^2), $\bar{\nu}_e$ energies and the short baseline $L \cong 60$ km we are interested in.

where $\Delta m_{\odot}^2 = \Delta m_{21}^2$ and $a_{\text{NH(IH)}}^2 = \sin^2 \theta_{12} (\cos^2 \theta_{12})$. For the atmospheric neutrino mass squared difference Δm_{atm}^2 in the case of NH (IH) spectrum we have $\Delta m_{\text{atm}}^2 = \Delta m_{31}^2 (\Delta m_{23}^2)$. The properties of the $\bar{\nu}_e$ survival probability $P_{\bar{e}\bar{e}}^{\text{NH(IH)}}$ have been discussed in detail in [49, 50]. We only note here that $P_{\bar{e}\bar{e}}^{\text{NH(IH)}}$ depends neither on the angle θ_{23} associated with the atmospheric neutrino oscillations, nor on the CP violating phase δ in the PMNS matrix. The fact that $\cos 2\theta_{12} \neq 0$, $\cos 2\theta_{12} \geq 0.26$ (at 3σ), opens up the possibility to get information about the neutrino mass spectrum if $\sin^2 2\theta_{13} \neq 0$: $P_{\bar{e}\bar{e}}^{\text{IH}} - P_{\bar{e}\bar{e}}^{\text{NH}} \propto \cos 2\theta_{12} \sin^2 2\theta_{13}$. This can be done, in principle, by studying the deformations of the observed event spectrum due to the $\bar{\nu}_e$ survival probability [49].

The detector energy resolution is taken into account assuming it has the standard Gaussian form:

$$R(E, E_m) = \frac{1}{\sqrt{2\pi}\sigma} \exp\left(-\frac{(E_m - E)^2}{2\sigma^2}\right). \quad (2.5)$$

Here E_m is the observed neutrino energy. We have $E_m - E = E_{\text{vism}} - E_{\text{vis}}$, where E_{vism} is the measured e^+ energy. The error for a scintillator detector is dominated by the photoelectron statistics, and hence σ/E_{vis} is proportional to $1/\sqrt{E_{\text{vis}}}$. We consider resolutions (i.e., σ/E_{vis}) in the range of $2\%/\sqrt{E_{\text{vis}}} - 4\%/\sqrt{E_{\text{vis}}}$.

Further, we take into account the energy scale uncertainty of the detector by considering an energy scale shrink/expansion both with and without energy dependence. This is parametrized as

$$E'_m = (1 + a)E_m + b, \quad (2.6)$$

where E_m is the neutrino energy after smearing and E'_m is the measured neutrino energy after including both the smearing and energy scale uncertainty. The parameters a and b define the shrink/expansion and the shift of the energy scale, respectively. The parameter a is taken to be 1% (unless otherwise specified) for the energy independent case, and 1% of E_m (i.e., $a = 0.01E_m$) for the energy dependent case.⁵ Rigorously, in the energy dependent case, a could have the form $a = cE_m + d$, corresponding to a combination of a non-linear and a linear dependence of E'_m on E_m . However, it will be shown later that considering an energy dependent and an energy independent scale uncertainty simultaneously in this way (c, d non-zero) has the same effect as considering only an energy dependent scale uncertainty (c non-zero, d zero).

The measured event rate spectrum, as a function of L/E_m , is thus given by

$$N(L/E_m) = \int R(E, E_m) \phi(E) \sigma(\bar{\nu}_e p \rightarrow e^+ n; E) P_{\bar{e}\bar{e}}^{\text{NH(IH)}} dE, \quad (2.7)$$

where $\phi(E)$ is the $\bar{\nu}_e$ flux spectrum, $\sigma(\bar{\nu}_e p \rightarrow e^+ n; E)$ is the inverse β -decay cross-section and $P_{\bar{e}\bar{e}}^{\text{NH(IH)}}$ is the $\bar{\nu}_e$ survival probability defined earlier.

The final statistics (total number of events) is a product of the event rate, the reactor power, the detector active mass and exposure time. The exposure is thus expressed in

⁵Accounting for the energy scale uncertainty on E_{vism} leads to an additional shift in E'_m which, however, does not have an effect on the spectrum features distinguishing between the NH and IH neutrino mass spectra (see subsections 3.1 and 3.2).

the unit kT GW yr. The KamLAND-like large underwater detector planned within the project Hanohano [91], can have a mass of up to ~ 10 kT and use a reactor having a power of ~ 5 GW. Hence we consider exposures in the range of 200-800 kT GW yr. A 100% efficiency of the detector is assumed. This gives, for example, a statistics of about 10^4 events (with oscillations) when an exposure of 200 kT GW yr is considered. Because of the high statistics, the geo-neutrino flux background at lower energies becomes insignificant [50] and it is possible to use the relatively low visible energy threshold of $E_{\text{visth}} = 1.0$ MeV mentioned earlier.

In the statistical analysis we take into account the systematic uncertainties relevant to a detector of the type assumed by us. We consider 5 sources of systematic errors (3 related to the detector and 2 due to the geo-neutrino flux) [51, 52]:

- i) The efficiency error, or the uncertainty in the predicted event rate, which can be between 1 to 5 %.
- ii) The uncertainty in the detector energy resolution estimation, which can be up to 10 %.
- iii) The energy scale uncertainty, which is around 1 %.
- iv) The uncertainty in the total detectable geo-neutrino flux.
- v) The uncertainty in the ratio of the geo $\bar{\nu}_e$ fluxes from the decays of U-238 and Th-232.

We find during the course of the study that the effects of the indicated systematic and geo-neutrino uncertainties on the neutrino mass hierarchy sensitivity are not significant.

Finally, we comment on the prospects of high precision determination of the neutrino oscillation parameters which serve as input in our analysis. The oscillation parameters Δm_{21}^2 , $\sin^2 \theta_{12}$ and $|\Delta m_{31}^2|$ are determined by the existing data with a 3σ error of approximately 9%, 17% and 15%, respectively. These parameters can (and very likely will) be measured with much higher accuracy in the future. The highest precision in the determination of $|\Delta m_{31}^2|$ is expected to be achieved in the next several years from the studies of ν_μ -oscillations in the T2K experiment with Super-Kamiokande detector (T2K (SK)) [75]: if the true $|\Delta m_{31}^2| = 2.5 \times 10^{-3} \text{ eV}^2$ (and true $\sin^2 \theta_{23} = 0.5$), the uncertainty in $|\Delta m_{31}^2|$ is estimated to be reduced in this experiment to 10^{-4} eV^2 or 4% at 90% C.L. [75–77]. The Fermilab-Homestake beam experiment (LBNE) is expected to reduce this error to less than 3% at 90% C.L. [78]. Further, reactor antineutrino experiments themselves may be able to provide a determination of $|\Delta m_{31}^2|$ with an uncertainty of approximately 1% at 1σ , or (3–4)% at 3σ [50–52]. In what concerns the CHOOZ angle θ_{13} , three reactor $\bar{\nu}_e$ experiments with baselines $L \sim (1-2)$ km, which could improve the current limit by a factor of (5–10), are under preparation: Double-CHOOZ [79], Daya-Bay [80, 81] and RENO [82] (see also [42]). The most precise measurement of Δm_{21}^2 could be achieved [83] using Super-Kamiokande doped with 0.1% of gadolinium (SK-Gd) for detection of reactor $\bar{\nu}_e$ [84]: getting the same flux of reactor $\bar{\nu}_e$ as KamLAND, the SK-Gd detector will have approximately 43 times bigger $\bar{\nu}_e$ -induced event rate than KamLAND. After 3 years of data-taking with SK-Gd, Δm_{21}^2 could be determined with an error of 3.5% at 3σ [83]. A

dedicated reactor $\bar{\nu}_e$ experiment with a baseline $L \sim 60$ km, tuned to the minimum of the $\bar{\nu}_e$ survival probability, could provide the most precise determination of $\sin^2 \theta_{12}$ [85–87]: with statistics of ~ 60 kT GW yr and systematic error of 2% (5%), $\sin^2 \theta_{12}$ could be measured with an error of 6% (9%) at⁶ 3σ [85–87].

3 The effects of energy smearing and energy scale uncertainty on the reactor $\bar{\nu}_e$ event rate and Fourier spectra

In this section we investigate in detail how the inclusion of the detector energy resolution and/or the energy scale uncertainty affects the reactor $\bar{\nu}_e$ event spectra, the Fourier spectra and hence the hierarchy sensitivity. For the detector’s energy resolution we use the Gaussian form given in eq. (2.5). We consider an energy scale shrink/expansion both with and without energy dependence, which is parametrized in the form specified in eq. (2.6). As we have already indicated, the parameter a in eq. (2.6) is taken to be 1% (unless otherwise specified) for the energy independent case, and 1% of E (i.e. a linear dependence on energy) for the energy dependent case.

3.1 Behaviour of the event rate spectrum

Figure 1 illustrates the changes of the reactor event rate spectrum in the case of $\bar{\nu}_e$ oscillations when one varies the energy resolution of the detector. This is done for both the normal and inverted hierarchies, without including the effects of the energy scale shift. The spectrum plotted in figure 1 is the normalized to 1 reactor $\bar{\nu}_e$ event rate spectrum:

$$f(L/E_m) = \frac{N(L/E_m)}{\int_{(L/E_m)_{\min}}^{(L/E_m)_{\max}} N(x) dx}, \tag{3.1}$$

where $(L/E_m)_{\min} = 5000$ Km/GeV, $(L/E_m)_{\max} = 32000$ Km/GeV, and $N(L/E_m)$ is given by eq. (2.7). Figures (a), (b) and (c) show the spectrum $f(L/E_m)$ without energy smearing (i.e. assuming perfect detector energy resolution), with a realistic smearing of 3% and with a large smearing of 20%, respectively. This and the subsequent event rate spectrum figures are obtained for $\sin^2 2\theta_{13} = 0.1$. The figures clearly show the effect of the energy resolution: the spectrum is slightly “flattened” towards the higher values of L/E_m in the case of resolution of 3% as compared to the unsmear spectrum; it is smeared throughout and the hierarchy sensitivity is completely lost over almost the entire L/E range if the detector’s energy resolution is as poor as 20%.

Figures 2 and 3 show the behaviour of the reactor $\bar{\nu}_e$ event rate spectrum when the detector resolution and/or the energy scale uncertainty are taken into account.

In figure 2, the spectrum with an energy smearing of 3% and an energy-independent expand/shrink is plotted, for both the cases of an expansion in energy scale, corresponding to $a = 1\%$, $b = 0.01$ MeV, and a shrink in energy scale, corresponding to $a = -1\%$, $b = -0.01$ MeV. The event spectra are seen to shift to the left and to the right, respectively.

⁶The inclusion of the current uncertainty in θ_{13} ($\sin^2 \theta_{13} < 0.05$) in the analysis increases the quoted errors by (1–3)% to approximately 9% (12%) [85–87].

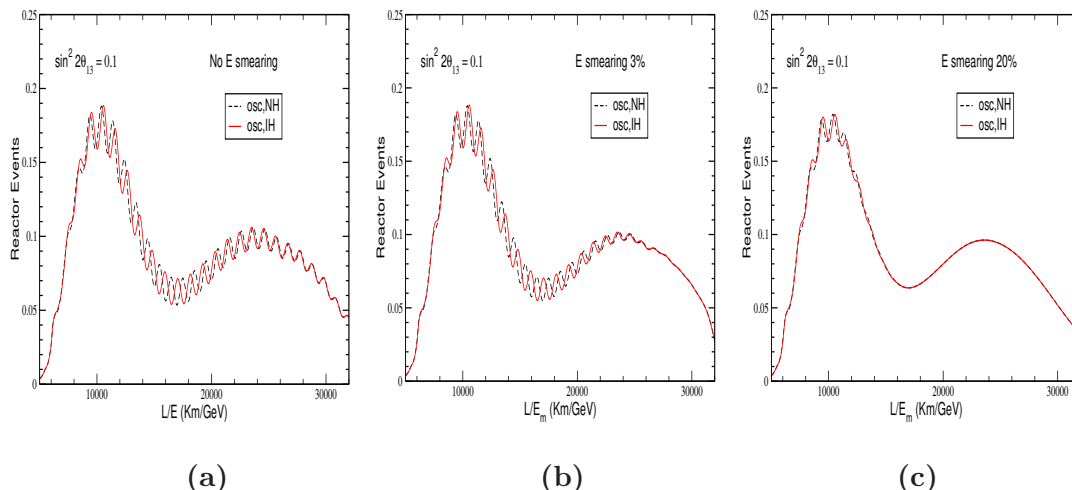


Figure 1. Reactor event rate vs L/E_m for normal and inverted hierarchies, for (a) ideal energy resolution, (b) 3% energy resolution and (c) 20% energy resolution of the detector.

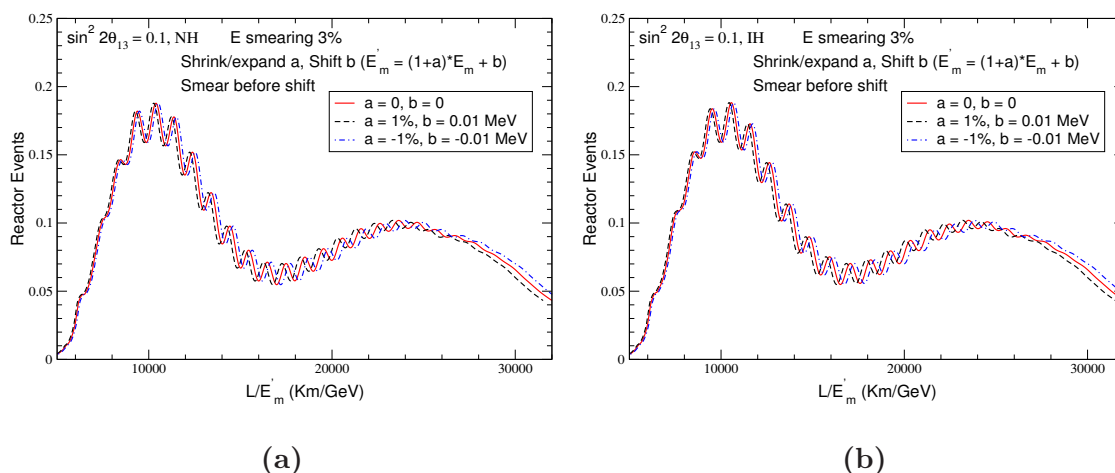


Figure 2. (a) Reactor event rate vs L/E'_m for normal hierarchy, 3% energy resolution of the detector and an energy-independent uncertainty (shrink/expansion and shift) in the energy scale. The energy scale shift is performed on the neutrino energy E_m after taking smearing into account. (b) The same as (a) for inverted hierarchy.

In figure 3 we plot the same spectra for energy-dependent expansion and shrink. The displacements in the spectra are seen to be larger in this case, and for this value of the expansion/shrink it leads to an effective flipping of the maxima/minima in the spectrum, as compared to the spectrum without shrink/expansion. Note that the effect is the same for the normal and inverted hierarchies. The changes in the event spectrum can be shown to be identical with those without energy smearing for both energy-independent and energy-dependent scale shifts.

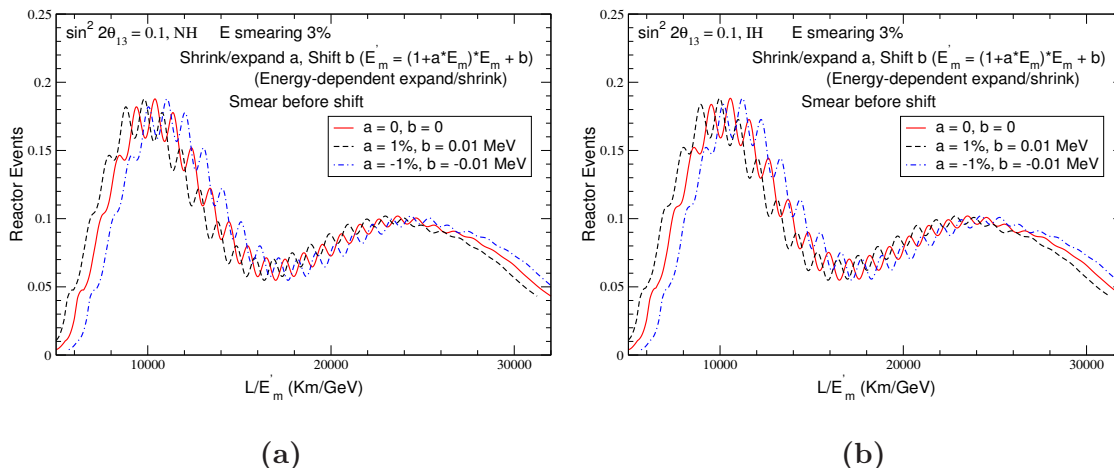


Figure 3. (a) Reactor event rate vs L/E'_m for normal hierarchy, 3% energy resolution of the detector and an energy-dependent uncertainty (shrink/expansion and shift) in the energy scale. The energy scale shift is performed on the neutrino energy E_m after taking smearing into account. (b) The same as (a) for inverted hierarchy.

3.2 Fourier analysis of the reactor $\bar{\nu}_e$ event rate spectrum

The Sine and Cosine Fourier Transforms of the reactor $\bar{\nu}_e$ event rate spectrum are computed as a function of the “frequency” δm^2 , varied in the range $2 \times 10^{-3} \text{ eV}^2$ to $2.8 \times 10^{-3} \text{ eV}^2$, using the best-fit values $|\Delta m_{31}^2| = 2.4 \times 10^{-3} \text{ eV}^2$ and $\Delta m_{21}^2 = 7.6 \times 10^{-5} \text{ eV}^2$. The expressions for the Fourier Transforms used by us read [53, 54]:

$$FCT(\omega) = \int_{(L/E_m)_{\min}}^{(L/E_m)_{\max}} f(L/E) \cos(\omega L/E) d(L/E), \quad (3.2)$$

$$FST(\omega) = \int_{(L/E_m)_{\min}}^{(L/E_m)_{\max}} f(L/E) \sin(\omega L/E) d(L/E). \quad (3.3)$$

Here $\omega = 2.54 \times \delta m^2 [eV^2]$, where δm^2 is in units of eV^2 , and L/E is in units of km/GeV .

The values $|\Delta m_{31}^2| = 2.4 \times 10^{-3} \text{ eV}^2$ and $\Delta m_{21}^2 = 7.6 \times 10^{-5} \text{ eV}^2$ appear in the normalised reactor $\bar{\nu}_e$ event rate spectrum $f(L/E)$. Hence, in the Fourier spectrum there is modulation due to both these frequencies. The modulation due to Δm_{31}^2 occurs near $\delta m^2 = 2.4 \times 10^{-3} \text{ eV}^2$, while that due to Δm_{21}^2 occurs near $\delta m^2 = 7.6 \times 10^{-5} \text{ eV}^2$. The values of the other neutrino oscillation parameters used in the calculations are $\sin^2 2\theta_{12} = 0.87$ and $\sin^2 2\theta_{13} = 0.1$ (unless otherwise stated).

According to [53, 54], the main features in the FCT and FST spectra that allow to distinguish between the two types of neutrino mass spectrum are:

- (a) In the FCT spectrum, $(RV - LV)$ has opposite signs for the NH and IH spectra, where RV and LV are the amplitudes of the right and left “valleys”, i.e., of the minima located closest (i.e., immediately) to the right (RV) and to the left (LV) of the absolute modulation maximum, in the Fourier spectra. The right “valley” is deeper than the left “valley” for the NH spectrum, and *vice versa* for the IH spectrum.

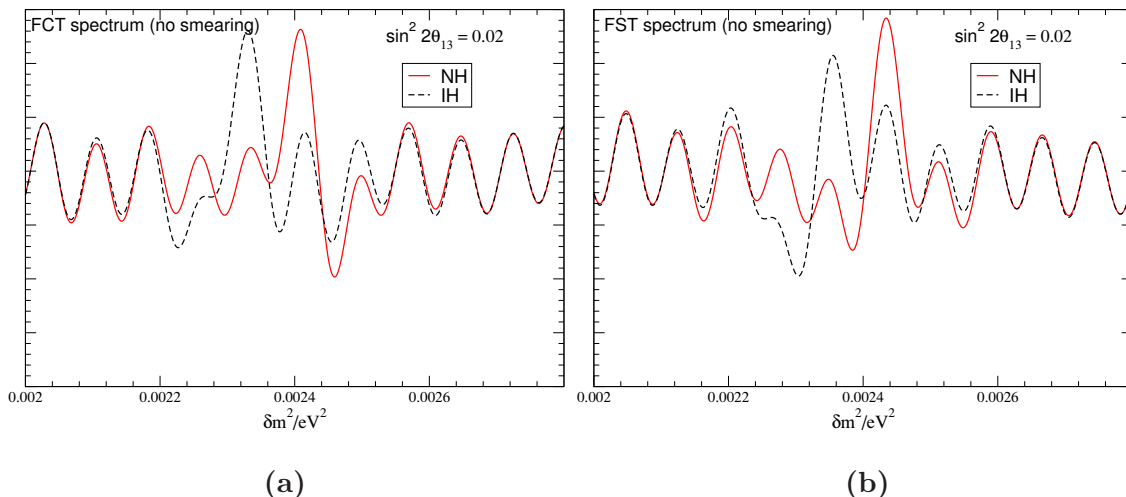


Figure 4. (a) Fourier cosine transformed (FCT) reactor $\bar{\nu}_e$ event rate spectrum vs δm^2 with power (y-axis) in arbitrary units, for $\sin^2 2\theta_{13} = 0.02$, normal hierarchy and inverted hierarchy, ideal energy resolution of the detector and no energy scale uncertainty. (b) Fourier sine transformed (FST) reactor $\bar{\nu}_e$ event rate spectrum vs δm^2 with power (y-axis) in arbitrary units, for $\sin^2 2\theta_{13} = 0.02$, normal hierarchy and inverted hierarchy, ideal energy resolution of the detector and no energy scale uncertainty.

(b) In the FST spectrum, $(P - V)$ has opposite signs for the NH and IH spectra, where P and V are the amplitudes of the absolute modulation maximum (“peak”) and of the absolute modulation minimum (“valley”) in the two event rate spectra. The amplitude of the “peak” is bigger than the amplitude of the “valley” for the NH spectrum, and *vice versa* for the IH spectrum.

The differences between the event rate spectra in the NH and IH cases can thus be quantified by the following two asymmetries [53, 54]:

$$RL = \frac{RV - LV}{RV + LV}, \quad (3.4)$$

for the FCT spectrum, and

$$PV = \frac{P - V}{P + V}, \quad (3.5)$$

for the FST spectrum. The RL and PV asymmetry features discussed above are illustrated in figure 4.

We have analyzed the effects of the detector’s energy resolution and energy scale uncertainty on the hierarchy-sensitive features of the FCT and FST spectra. Both the cases of energy-independent and energy-dependent energy scale uncertainty (“shrink/expansion”) have been considered. The magnitude of the shrink (expansion) was assumed to be (-1%) ((+1%)).

Our results are illustrated in figures 5–9, in which we show the FCT and FST spectra, corresponding to the NH and IH neutrino mass spectra, for different combinations of the detector’s energy resolution and forms of the energy scale uncertainty. The figures are

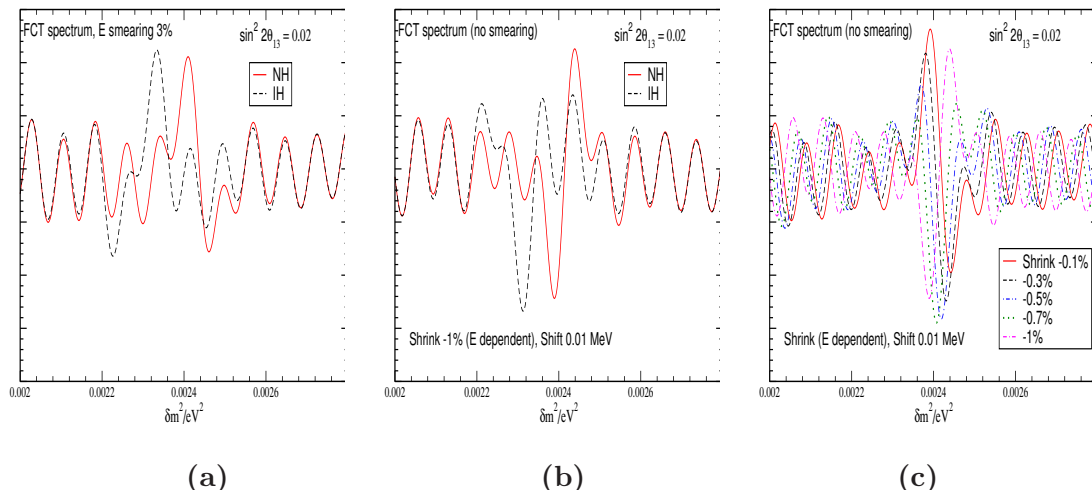


Figure 5. (a) Fourier cosine transformed (FCT) reactor $\bar{\nu}_e$ event rate spectrum vs δm^2 with power (y-axis) in arbitrary units, for $\sin^2 2\theta_{13} = 0.02$, normal hierarchy and inverted hierarchy, 3% energy resolution of the detector and no energy scale uncertainty. (b) Fourier cosine transformed (FCT) reactor $\bar{\nu}_e$ event rate spectrum vs δm^2 with power (y-axis) in arbitrary units, for $\sin^2 2\theta_{13} = 0.02$, normal hierarchy and inverted hierarchy, ideal energy resolution of the detector and energy-dependent uncertainty (shrink and shift) in the energy scale. (c) FCT spectrum for $\sin^2 2\theta_{13} = 0.02$, normal hierarchy, ideal energy resolution of the detector and different values of energy-dependent uncertainty in the energy scale.

obtained for $\Delta m_{31}^2(IH) = -\Delta m_{32}^2(NH)$, $\sin^2 2\theta_{13} = 0.02$, and the best-fit values of all other neutrino oscillation parameters.

Comparing the respective curves in figures 5, 6, 7 and 8 demonstrates that with an energy-independent “shrink” performed on the measured energy (after smearing), the Fourier spectra get simply displaced to the left in all cases, with no change in the overall shape of the spectra. The shrink in the event versus energy spectrum leads to an “expansion” in the event versus L/E_m spectrum, and as a consequence one obtains a given feature (maximum, minimum) at a smaller value of the oscillation frequency δm^2 . This behaviour is accentuated if higher values of “shrink” are considered. This leads to an overall left shift in the Fourier (frequency) spectra. Since the sensitivity to the hierarchy in the Fourier spectra is related to the relative positions and the amplitudes of the maxima and minima of the spectra, the indicated changes do not affect results on the hierarchy sensitivity. In the case of an energy-dependent shrink, however, the change in the Fourier spectra is more complicated and the shape gets distorted, as the figures clearly show. This behaviour in both cases (energy-dependent or energy-independent shrink) is identical to the change in the corresponding spectra due only to an energy scale shift and no energy smearing, as observed by comparing figures 4, 5 and 7. The above comments hold true for both the FCT and FST spectra and for both the normal and inverted hierarchies.

An energy-independent energy scale “expansion” of 1% gives a uniform right displacement to the Fourier spectra, as expected. This is because the event versus L/E_m spectrum shrinks with an expansion in the energy spectrum, leading to a shift of the Fourier spectral

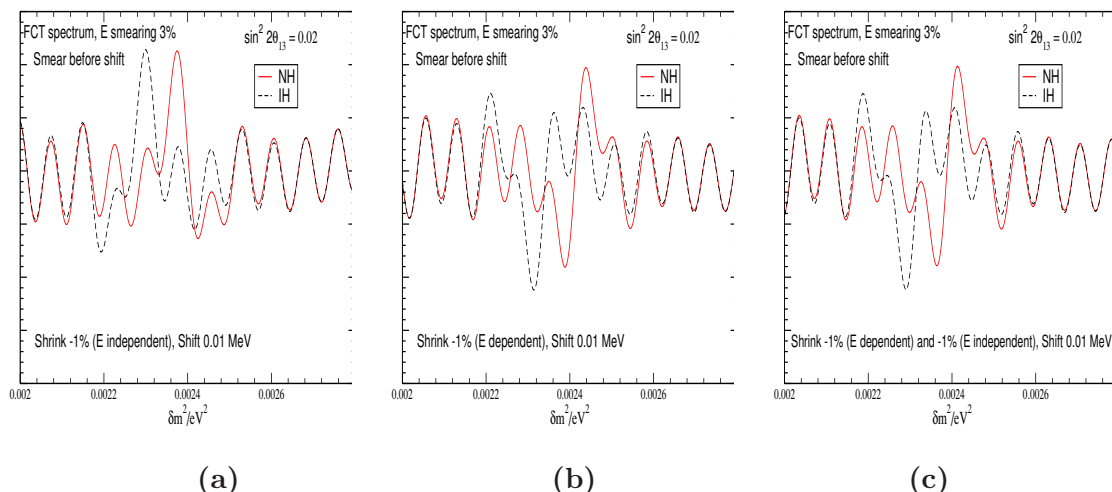


Figure 6. (a) Fourier cosine transformed (FCT) reactor $\bar{\nu}_e$ event rate spectrum vs δm^2 with power (y-axis) in arbitrary units, for $\sin^2 2\theta_{13} = 0.02$, normal hierarchy and inverted hierarchy, 3% energy resolution of the detector and energy-independent uncertainty (shrink and shift) in the energy scale. The energy scale shift is performed on the neutrino energy E_m after taking smearing into account. (b) The same as in (a), but for energy-dependent uncertainty (shrink and shift) in the energy scale. (c) The same as in (a) and (b), but for a combination of an energy-dependent and energy-independent uncertainty (shrink and shift) in the energy scale.

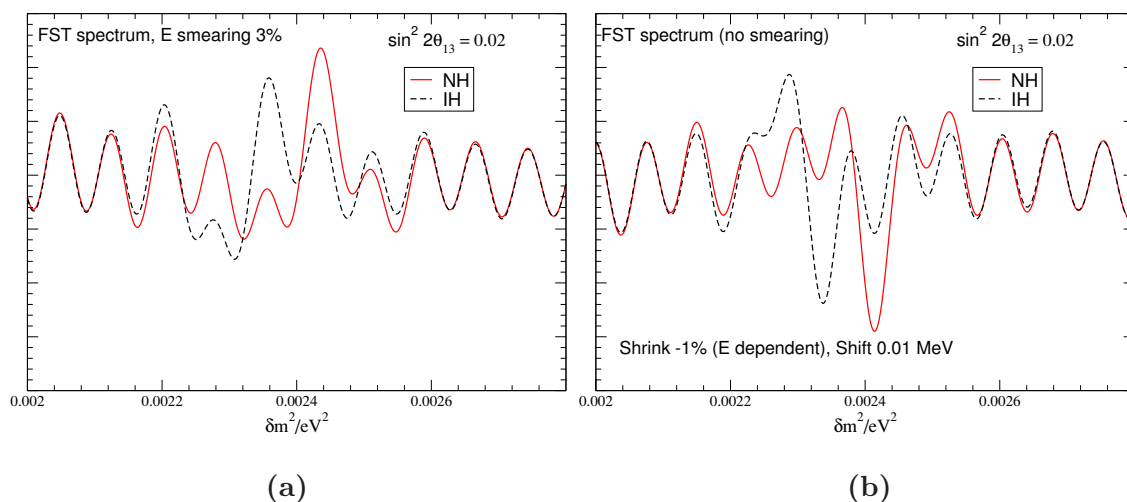


Figure 7. (a) Fourier sine transformed (FST) reactor $\bar{\nu}_e$ event rate spectrum vs δm^2 with power (y-axis) in arbitrary units, for $\sin^2 2\theta_{13} = 0.02$, normal hierarchy and inverted hierarchy, 3% energy resolution of the detector and no energy scale uncertainty. (b) Fourier sine transformed (FST) reactor $\bar{\nu}_e$ event rate spectrum vs δm^2 with power (y-axis) in arbitrary units, for $\sin^2 2\theta_{13} = 0.02$, normal hierarchy and inverted hierarchy, for ideal energy resolution of the detector and energy-dependent uncertainty (shrink and shift) in the energy scale.

features to a higher frequency. With energy-dependent expansion of the measured energy scale, the spectrum shape is again changed (see figure 9).

As discussed above, the distinguishing feature of the NH and IH neutrino mass spectra

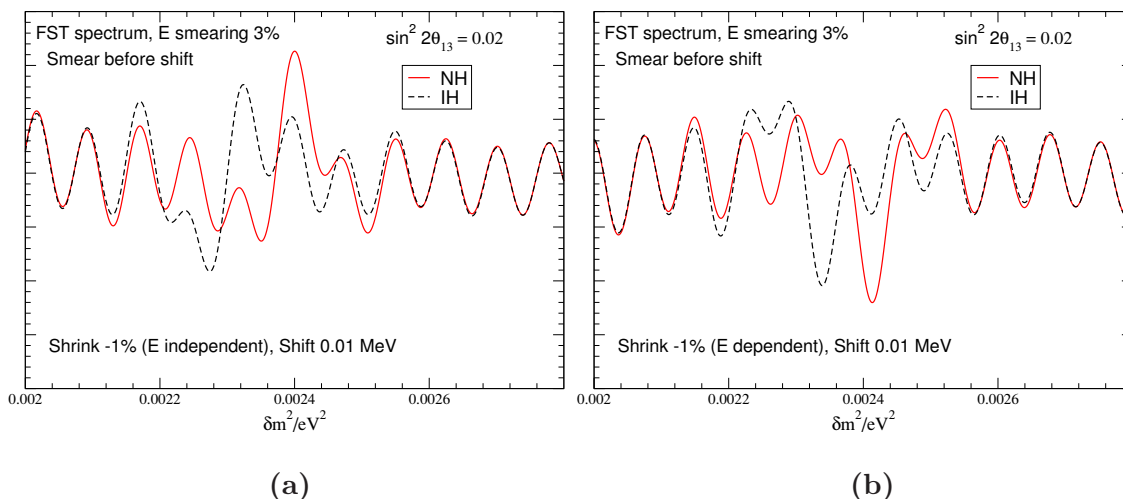


Figure 8. (a) Fourier sine transformed (FST) reactor $\bar{\nu}_e$ event rate spectrum vs δm^2 with power (y-axis) in arbitrary units, for $\sin^2 2\theta_{13} = 0.02$, normal hierarchy and inverted hierarchy, for 3% energy resolution of the detector and energy-independent uncertainty (shrink and shift) in the energy scale. The energy scale shift is performed on the neutrino energy E_m after taking smearing into account. (b) The same as in a, but for energy-dependent uncertainty (shrink and shift) in the energy scale.

in the FCT spectrum, according to [53, 54], is the sign of the asymmetry RL defined in eq. (3.4): we have $RL > 0$ ($RV > LV$) in the case of normal hierarchy and $RL < 0$ ($RV < LV$) for the inverted hierarchy. In the case of the FST spectrum, it was proposed in [53, 54] to distinguish between the normal and inverted hierarchy neutrino mass spectra by the sign of the asymmetry PV defined in eq. (3.5): one has $PV > 0$ ($P > V$) in the NH case and $PV < 0$ ($P < V$) if the IH spectrum is realized. On the basis of our analysis we can make the following observations.

FCT spectrum.

- Comparing figure 4(a) (no smearing, no scale shift) with figure 5(a) (3% smearing, no scale shift), the sign feature of the asymmetry $RL = (RV - LV)/(RV + LV)$, distinguishing between the NH and IH cases, is seen to be retained with a smearing of 3%, with a somewhat reduced (increased) absolute magnitude of the asymmetry RL in the NH (IH) case (we find $RL(NH) = 0.39$, $RL(IH) = -0.11$ in figure 4(a) and $RL(NH) = 0.20$, $RL(IH) = -0.35$ in figure 5(a)).
- Comparing figure 4(a) with figure 5(b) (no smearing, energy scale shift with energy-dependent shrink of 1%), the RL asymmetry feature distinguishing between the two hierarchies is no longer present with the inclusion of an energy-dependent energy scale shrink. Instead, the absolute modulation maxima in the NH and IH spectra appear to be replaced by absolute modulation minima, while the adjacent valleys (minima) are replaced by adjacent peaks (maxima). We can define a quantity

$$RLP = \frac{RP - LP}{RP + LP}, \tag{3.6}$$

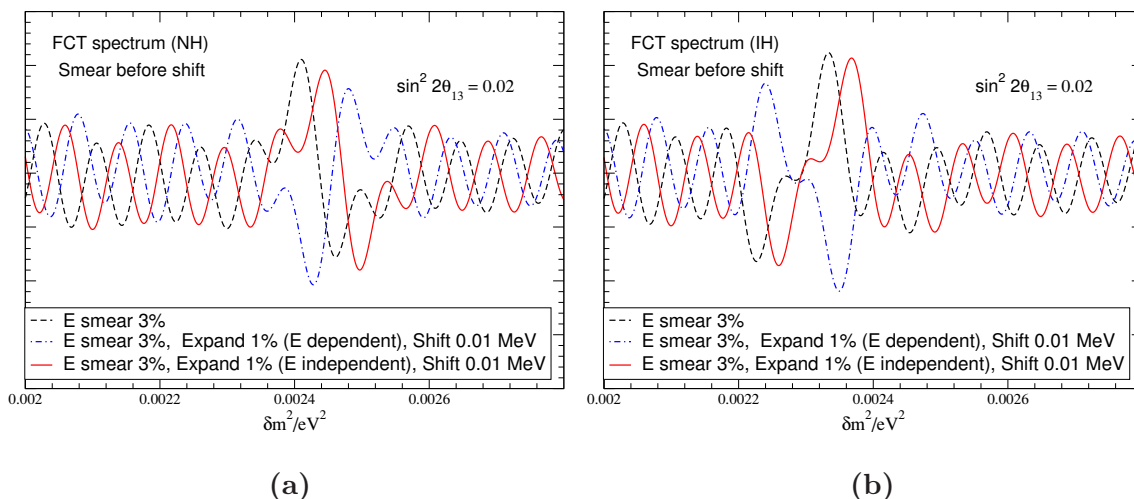


Figure 9. (a) Fourier cosine transformed (FCT) reactor $\bar{\nu}_e$ event rate spectrum vs δm^2 with power (y-axis) in arbitrary units, for $\sin^2 2\theta_{13} = 0.02$, normal hierarchy, 3% energy resolution of the detector and for both energy-dependent and energy-independent uncertainty (expansion and shift) in the energy scale. The energy scale shift is performed on the neutrino energy E_m after taking smearing into account. (b) The same as (a) for inverted hierarchy.

where RP and LP are the amplitudes of the right and left peaks adjacent to the absolute modulation minima. This is seen to have a significant positive value for the NH spectrum, and a much smaller value close to zero for the IH spectrum.

This behaviour can be explained on the basis of figure 3 (the unsmeared reactor event spectrum as a function of L/E and with an energy-dependent scale shrink), and figure 5(c), in which the FCT spectrum for NH (without smearing) is plotted for different values of the energy-dependent shrink factor, varying from 0.1% ($a = 0.001 \times E_m$ in eq. (2.6)) to 1% ($a = 0.01 \times E_m$). It may be observed that there is a gradual left-shift in the FCT spectrum with an increase in the shrink factor, as well as a change in its shape, with a progressive drop in the amplitudes of the maxima and an increase in the amplitudes of the minima in the modulation region. This shift leads to what looks like a flipping of the maxima and minima when the shrink reaches a value of 1%. Note that this is not an actual inversion, but a feature caused by the left-shift and shape change of the spectrum. We have observed that in the corresponding event spectrum (figure 3), there is a large right-shift due to the energy-dependent shrink, which leads to an effective inversion of the maxima and minima (as compared to the spectrum without shrink) for this value of the shrink factor. This is reflected in the left-shift and change in shape of the Fourier spectrum, which leads to an effective flipping of the modulation maxima and minima for a shrink of 1% or more (note that this is a continuous conversion as the value of the shrink increases).

It may be pointed out that since this is a continuous change in the shape of the Fourier spectrum, the RL asymmetry feature (eq. (3.4)) is retained till a value of the energy-dependent shrink upto about 0.3%, while the RLP asymmetry feature in the

changed spectrum (eq. (3.6)) becomes effective at values of about 0.7% or larger. For intermediate values of the shrink factor, it is difficult to pinpoint a specific asymmetry feature.

- Comparing figure 5(a) with figure 6(a) (3% smearing, scale shift with energy-independent shrink of 1% performed after smearing), the energy-independent shrink is seen to leave the hierarchy-sensitive feature almost unchanged, as expected from the preceding discussion.
- Comparing figure 5(a) with figure 6(b) (3% smearing, scale shift with energy-dependent shrink of 1% performed after smearing), the energy-dependent shrink is again observed to flip the modulation maxima to minima (as in figure 5(b)), and the hierarchy-sensitive feature can again be defined as RLP , which in this case is still large and positive for the NH spectrum and has a small negative value for the IH spectrum (we have $RLP(NH) = 0.40$, $RLP(IH) = -0.14$ in figure 6(b)).
- Comparing figure 6(a) and 6(b) with figure 6(c) (3% smearing, scale shift with energy-dependent shrink of 1% and energy-independent shrink of 1% performed after smearing), it is seen that the resulting FCT spectrum is almost identical to the spectrum in figure 6(b) obtained with only an energy-dependent shrink factor of 1%. This is because, as noted earlier, the energy-independent shrink factor leaves the spectrum almost unchanged (figure 6(a)). Hence a combination of a linear and a non-linear scale uncertainty leads to the same effects as a non-linear scale uncertainty. A similar behaviour is observed in the FST spectrum.

FST spectrum.

- Comparing figure 4(b) (no smearing, no scale shift) with figure 7(a) (3% smearing, no scale shift), the hierarchy-sensitive feature of the asymmetry $PV = (P - V)/(P + V)$ is seen to be retained. This feature is reflected in a large positive value of the asymmetry PV for the NH spectrum and a value close to zero for the IH spectrum (we have $PV(NH) = 0.32$, $PV(IH) = 0.04$ in figure 4(b), and $PV(NH) = 0.41$, $PV(IH) = 0.07$ in figure 7(a)).
- Comparing figure 4(b) with figure 7(b) (no smearing, scale shift with energy-dependent shrink of 1%), we see that the PV asymmetry features corresponding to the NH and IH spectra are not present when the energy-dependent shrink is taken into account. Now the FST spectra show a behaviour similar to that of the FCT spectra with an energy-dependent shrink (figure 5(b) and figure 6(b)), i.e. the absolute modulation maxima in the NH and IH cases are effectively replaced by absolute modulation minima and the adjacent right and left (minima) valleys are replaced by right and left (maxima) peaks, RP and LP . Here the quantity RLP is close to zero for the NH spectrum and is significantly different from zero and negative for the IH spectrum. This behaviour is explained in the same way as for the FCT spectrum: it also appears for values of the shrink of about 0.7% or larger, while the PV asymmetry feature is retained for very small values of the shrink of upto about 0.3%.

- Comparing figure 7(a) with figure 8(a) (3% smearing, scale shift with energy-independent shrink of 1% performed after smearing), the PV asymmetry feature, distinguishing between the NH and IH spectra, remains largely unchanged, as expected.
- Comparing figure 7(a) with figure 8(b) (3% smearing, scale shift with energy-dependent shrink of 1% performed after smearing), we see that features distinguishing between the NH and IH spectra in the case of a scale shift with an energy-dependent shrink of 1% are the same as in the unsmear case discussed above (when comparing figure 4(b) with figure 7(b)).

In the cases of energy-independent and energy-dependent energy scale expansion, the FCT and FST spectra exhibit the same features as those discussed above assuming energy-independent and energy-dependent energy scale shrink, respectively. For the FCT spectrum this is illustrated in figure 9. Comparing the curves with energy-dependent expansion in figure 9(a) and 9(b) shows that the RLP asymmetry feature is present. With an increase in the magnitude of the shrink/expansion uncertainty, the asymmetry features discussed above survive with a reduced amplitude, getting washed out if the uncertainty exceeds $\sim 5\%$.

The above properties of the Fourier spectra indicate that it should be possible, in principle, to extract information about the type of the spectrum the neutrino masses obey from the features present in the spectra, although the nature of the hierarchy-dependent features is changed in the case of an energy-dependent energy scale shrink/expansion.

3.3 The effect of the uncertainty of Δm_{31}^2 on the Fourier spectra

The effect of varying the atmospheric neutrino mass-squared difference over its error range, in general, causes a change in the magnitude of the hierarchy-sensitive asymmetry features of the Fourier spectra. More specifically we note the following.

- **FCT spectra.** Comparing the NH and IH FCT spectra for different values of Δm_{31}^2 over its uncertainty range, it can be seen that the RL asymmetry feature of the NH and IH spectra is completely changed in the case of an energy-dependent scale shrink/expansion. Instead, the RLP asymmetry feature discussed in the context of figure 5(b) and figure 6(b) appears. This feature is present throughout the considered range of Δm_{31}^2 , though the magnitude of the effect varies over the range.
- **FST spectra.** Comparing the NH and IH FST spectra, it can be seen that the PV asymmetry feature in the spectra is changed in the case of the energy-dependent energy scale shrink/expansion, and the RLP asymmetry feature comes into play, as earlier noted in connection with figure 7(b) and figure 8(b). It is present with different amplitudes throughout the considered range of Δm_{31}^2 .

4 χ^2 -analysis of the sensitivity to the type of the neutrino mass spectrum

In the present section we perform a full χ^2 -analysis of the sensitivity to the type of the neutrino mass spectrum of a “measured” reactor $\bar{\nu}_e$ spectrum. This allows us to take into

account in a systematic way the uncertainties in the knowledge of $|\Delta m_{\text{atm}}^2|$, θ_{13} , Δm_{21}^2 , θ_{12} , the uncertainty in the energy scale, the systematic and geo-neutrino uncertainties, as well as the effects of the detector energy resolution. As is well known, the uncertainties in the values of $|\Delta m_{\text{atm}}^2|$ and θ_{13} , in particular, play a crucial role in the sensitivity to the neutrino mass hierarchy.

We perform a binned χ^2 analysis which involves an optimization in binning, a marginalization over the relevant neutrino oscillation parameters, and incorporation of systematic errors by the method of pulls. We find that an energy scale shrink/expansion and/or shift at the level of $\sim 1\%$, even when energy-dependent, does not affect the sensitivity to the hierarchy, and that the inclusion of the systematic and geo-neutrino flux uncertainties has only a minimal effect on the sensitivity of interest. We present results for different values of $\sin^2 \theta_{13}$, the detector exposure and the energy resolution. A prior term is added to the sensitivity to take into account information from other experiments on parameter uncertainties, and it is shown that if the present error ranges are considered, this external information leads to only a slight improvement in the results.

In order to compute the hierarchy sensitivity by the χ^2 -method, it is necessary to have binned event data. For a set of "experimental" (observed) events $N_{ex}(i)$ and "theoretical" (predicted) events $N_{th}(i)$, the standard Gaussian definition of the least squares sum of binned data reads:

$$\chi_{\text{stat}}^2 = \sum_i \frac{[N_{ex}(i) - N_{th}(i)]^2}{N_{ex}(i)}, \quad (4.1)$$

where only the statistical error $\sigma_{\text{stat}} = \sqrt{N_{ex}(i)}$ is taken into account, and i denotes the bin label. We simulate the "experimental" spectrum N_{ex} for a fixed "test" or "true" hierarchy (performed with a normal hierarchy unless otherwise specified; the difference in results is minimal). All other parameters are also kept fixed at a set of "test" values in N_{ex} . The theoretical spectrum N_{th} is then generated with the *other* hierarchy, called the "wrong" hierarchy. The χ^2 thus obtained determines the confidence level at which the "wrong" hierarchy can be *excluded* (i.e., the " χ^2 sensitivity") given the "true" hierarchy, the set of values of all other parameters used and the given values of errors, uncertainties, detector resolution, exposure, etc.

Errors other than the σ_{stat} , like the flux and geo-neutrino uncertainties and systematic errors, can be included using the method of pulls. Also, a comprehensive χ^2 analysis requires a marginalization over the uncertainties in the neutrino oscillation parameters, which can be done by varying the parameters in the theoretical spectrum N_{th} and choosing the minimum value of χ^2 after taking into account this variation.

Optimization of bin number. Figure 10 shows the behaviour of the χ^2 sensitivity with an increase in the bin number. We plot in the figure the values of χ^2 with fixed neutrino parameters for an exposure of 200 kT GW yr, $\sin^2 2\theta_{13} = 0.05$, $\Delta_{31}(NH) = 0.0024$, $\Delta_{31}(IH) = -\Delta_{31}(NH) + \Delta_{21}$ and a detector resolution of 3%, for different numbers of L/E bins in the range $L/E = 5 - 32$ Km/MeV. The sensitivity is seen to improve dramatically with an improvement in the fineness of binning. However, the maximum bin number that

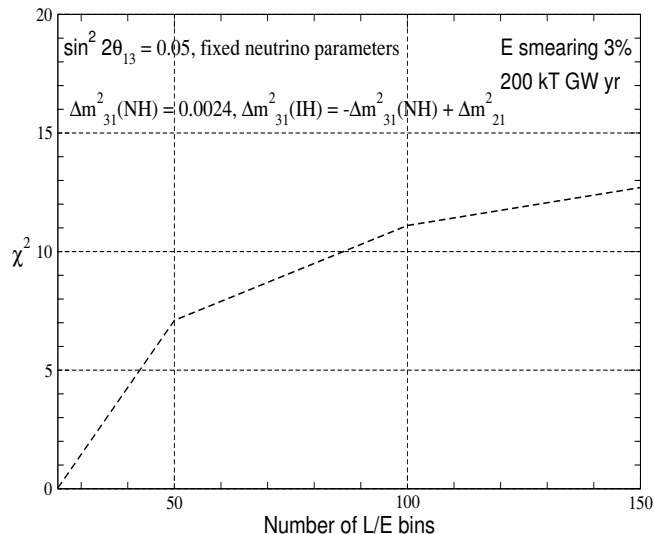


Figure 10. The hierarchy sensitivity $(\chi^2)_{\text{stat}}$ as a function of the number of L/E bins, for fixed neutrino oscillation parameters, $\sin^2 2\theta_{13} = 0.05$ and detector’s energy resolution of 3%, statistics of 200 kT GW yr, baseline of 60 Km and different L/E binnings in the range $L/E = 5 - 32$ Km/MeV.

can be used is restricted by the energy resolution of the detector. Hence, it becomes important to optimize the number of bins and choose a binning which is fine enough to give the best possible sensitivity while being consistent with the detector resolution.

In general, the bin width can be chosen to be of the same order as the resolution width, but not significantly smaller. Here, an energy resolution of 3% would mean a resolution width of $0.03 \times \sqrt{E_{\text{vis}}}$, or approximately 0.03 - 0.1 MeV, over the given energy range of $E = 1.8$ to 12 MeV. Hence we can choose to take approximately $10.2/0.07 = 145$ bins in this energy range. Therefore, we consider a 150-bin analysis. The no-oscillation unbinned reactor event spectrum is used to generate a binned spectrum of events (the product of the no-oscillation event spectrum and the oscillation probability) in L/E bins of width 0.18 Km/MeV, i.e. 150 bins in the given L/E range of 5 - 32 Km/MeV. The simulated "predicted" spectra are then used to calculate the χ^2 sensitivity.

Figures 11 and 12 show the 150-bin event spectrum for both the normal and inverted hierarchies, with or without energy smearing and energy scale shift, using the no-oscillation spectrum as the unbinned data. The figures are obtained for $\sin^2 2\theta_{13} = 0.05$ and a detector exposure of 200 kT GW yr. It can be seen that the NH and IH spectra show small differences through a greater part of the L/E range, which in a χ^2 analysis can give a significant result since the procedure adds up the contributions from all the bins. A smearing of 3% washes out the sensitivity in part of the L/E range, as expected. The energy scale shift/shrink is seen to affect both the NH and the IH spectra identically.

4.1 Parameter marginalization

For a realistic analysis, one needs to take into account the ranges of uncertainty of the neutrino oscillation parameters, since they are not known to infinite precision. In order

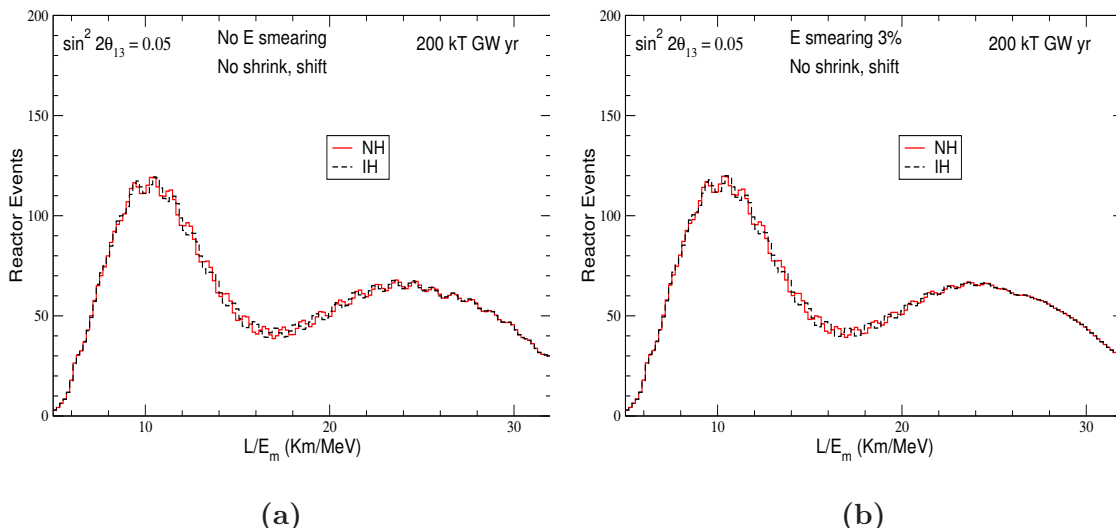


Figure 11. (a) Reactor event spectrum binned in 150 L/E_m bins for both the normal and inverted hierarchies, for $\sin^2 2\theta_{13} = 0.05$, ideal energy resolution of the detector (no smearing) and no energy scale shift. (b) The same as (a) for 3 % energy resolution of the detector.

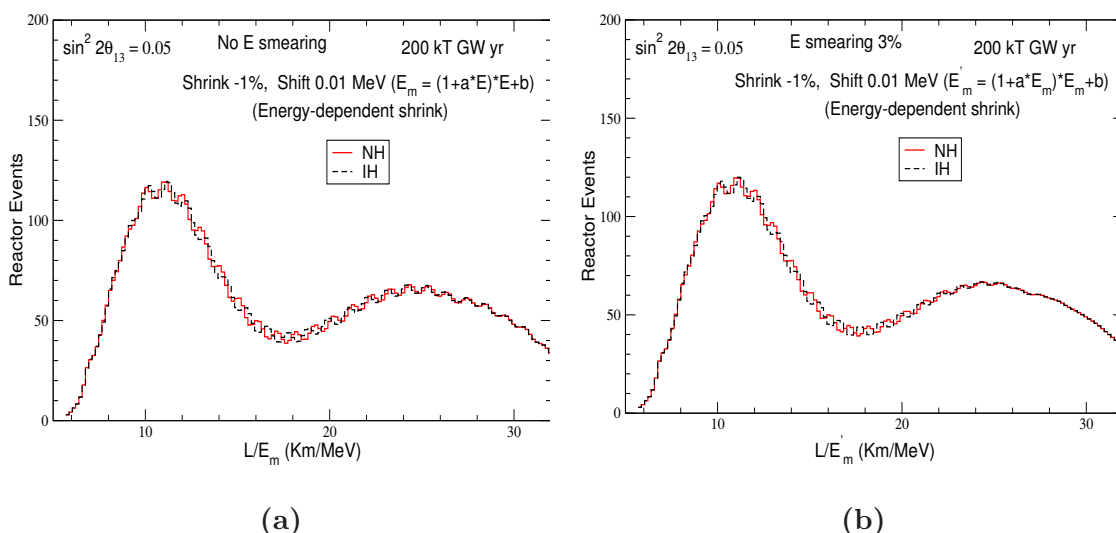


Figure 12. (a) Reactor event spectrum binned in 150 L/E_m bins for both the normal and inverted hierarchies, for $\sin^2 2\theta_{13} = 0.05$, for ideal energy resolution of the detector (no smearing) and an energy-dependent uncertainty (shrink/expansion and shift) in the energy scale. (b) The same as (a) for 3 % energy resolution of the detector.

to do this, the values of the parameters (ideally all the neutrino parameters) are fixed at certain input ("true") values in the "observed" event spectrum $N_{ex}(i)$ and varied over their present error ranges while computing the "theoretical" event spectrum $N_{th}(i)$, subsequently choosing the minimum value of χ^2 after including a full variation.

Practically, since the solar neutrino parameters θ_{12} and Δm_{21}^2 are already measured with a relatively high precision and the dependence of the oscillation probability on their

variation is rather weak, it usually suffices to marginalize over the parameters θ_{13} and $|\Delta m_{31}^2|$. We have checked that a marginalization over θ_{12} and Δm_{21}^2 over their present 3σ ranges ($\sin^2 \theta_{12} = 0.27 - 0.38$, $\Delta m_{21}^2 = 7.0 \times 10^{-5} - 8.3 \times 10^{-5}$) does not affect the results. Also, the fineness of binning in the parameters being varied during the process of marginalization needs to be optimized, since taking a coarse binning may give inaccurate results due to missing the actual point of minimal χ^2 , while making the binning more rigorous gives progressively improved results but also increases the computational time involved.

We consider the following error ranges for the two marginalized parameters: i) $|\Delta_{31}|$ is allowed to vary in the range $2.3 \times 10^{-3} - 2.6 \times 10^{-3} \text{ eV}^2$, and ii) $\sin^2 2\theta_{13}$ is varied from 0.0 to 0.15.

4.2 The precision on Δm_{atm}^2 and its effect on the hierarchy sensitivity

When an experiment determines the atmospheric mass-squared difference, assuming that it does not also simultaneously determine the hierarchy, the question arises of what exactly it measures. We know that by definition, when the hierarchy is normal, the magnitude of Δm_{31}^2 is greater than that of Δm_{32}^2 , since the third mass state lies above the states 1 and 2, while in the case of an inverted hierarchy, Δm_{32}^2 is greater in magnitude than Δm_{31}^2 , since the third state lies below the first two. So, if the experiment measuring the mass-squared difference does not know the hierarchy, it is not possible for it to measure the quantity $|\Delta m_{31}^2|$ or $|\Delta m_{32}^2|$. We can reasonably assume that it measures something in between, or an effective Δm_{atm}^2 which is blind to the hierarchy, i.e. $|\Delta m_{\text{atm}}^2(NH)| = |\Delta m_{\text{atm}}^2(IH)|$. This is, in general, a linear combination of Δm_{31}^2 and Δm_{32}^2 , i.e.

$$\Delta m_{\text{atm}}^2 = c\Delta m_{31}^2 + d\Delta m_{32}^2, \tag{4.2}$$

where c and d can vary from 0 to 1 and $c + d = 1$.

Now when we perform the χ^2 analysis for the hierarchy sensitivity, we require, as inputs from some experimental measurement, the range of uncertainty in the atmospheric mass-squared difference, as well as the values of Δm_{31}^2 and Δm_{32}^2 for both the normal and the inverted hierarchies, when computing the survival probability $P_{\bar{e}\bar{e}}$ in the two cases (the probability is the only neutrino parameter-dependent part in the event spectra N_{ex} and N_{th}). Hence we need to know how the magnitudes of Δm_{31}^2 and Δm_{32}^2 are related for the two hierarchies. From the definition of the measured Δm_{atm}^2 and the fact that it is equal in magnitude for NH and IH, it can be derived that the following relations hold:

$$\begin{aligned} |\Delta m_{31}^2(IH)| &= \Delta m_{31}^2(NH) - 2d\Delta m_{21}^2, \\ |\Delta m_{32}^2(IH)| &= \Delta m_{32}^2(NH) + 2c\Delta m_{21}^2, \end{aligned} \tag{4.3}$$

where c and d can vary from 0 to 1. In other words, the magnitude of $\Delta m_{31}^2(IH)$ (as derived from the measured mass-squared difference) can vary from anywhere between $\Delta m_{31}^2(NH)$ to $\Delta m_{31}^2(NH) - 2\Delta m_{21}^2$, while the magnitude of $\Delta m_{32}^2(IH)$ can be anywhere between $\Delta m_{32}^2(NH)$ to $\Delta m_{32}^2(NH) + 2\Delta m_{21}^2$.

In some cases (for specific experiments and measurements localized in specific regions of L/E) it is possible to pinpoint the exact linear combination being measured, since the

relevant 3-flavour probability expressions may be reducible (with certain approximations) to effective 2-flavour forms which then define an effective mass-squared difference as the argument [94].⁷ In our analysis, we assume the most general case of an input from an experiment where an unknown linear combination is being measured.

The hierarchy sensitivity depends on the difference between the survival probability $P_{\bar{e}\bar{e}}$ for the two hierarchies, since the χ^2 function is an artefact of this probability difference, averaged over L/E bins. For different values of the baseline L (i.e. different ranges of L/E), the $P_{\bar{e}\bar{e}}$ expression would give a minimized value of $\Delta P_{\bar{e}\bar{e}} = P_{\bar{e}\bar{e}}(NH) - P_{\bar{e}\bar{e}}(IH)$ for different values of $\Delta m_{31}^2(IH)$ and $\Delta m_{32}^2(IH)$ in $P_{\bar{e}\bar{e}}(IH)$ (fixing a $\Delta m_{31}^2(NH)$ and $\Delta m_{32}^2(NH)$ in $P_{\bar{e}\bar{e}}(NH)$). In general, the minimum of $\Delta P_{\bar{e}\bar{e}}$ would occur for a point $|\Delta m_{31}^2(IH)| < \Delta m_{31}^2(NH)$ and $|\Delta m_{32}^2(IH)| > \Delta m_{32}^2(NH)$, for the same reason as discussed above - this is how they are related in nature. So when performing the χ^2 analysis, in addition to marginalizing over the error range in Δm_{atm}^2 (and hence in both $\Delta m_{31}^2(NH)$ and $\Delta m_{31}^2(IH)$), the possible variation in $|\Delta m_{31}^2(IH)|$ relative to $\Delta m_{31}^2(NH)$ as defined by eq. (4.3) also has to be taken into account.

Thus, $|\Delta m_{31}^2(IH)|_{th}$ in the N_{th} spectrum is varied from $\Delta m_{31}^2(NH)$ to $\Delta m_{31}^2(NH) - 2\Delta m_{21}^2$, i.e. 0.0024 to 0.002248 as well as over the error range of $|\Delta m_{\text{atm}}^2|$ (which is at present 0.0021 - 0.0028 at 3σ). Extending the range of marginalization does not change our results. What we need to check is the value of the minimum χ^2 obtained during this variation, at which point of $|\Delta m_{31}^2(IH)|$ it occurs, and whether it is zero or negligibly small at any point in this range. It is found that (for the true value $\sin^2 2\theta_{13} = 0.05$ and a detector resolution of 4%, 200 kT GW yr exposure, and with a marginalization over θ_{13}), the minimum χ^2 is about 2, and occurs at about $|\Delta m_{31}^2(IH)|_{th} = 0.002387$, as can be seen in figure 13, which shows the values of χ^2 (with the above specifications) as a function of the magnitude of Δm_{31}^2 in the theoretical spectrum, choosing the hierarchy to be normal in N_{ex} and normal (dashed curve) or inverted (solid curve) in N_{th} .

This verifies that for the hierarchy sensitivity arising from the survival probability $P_{\bar{e}\bar{e}}$, in this L/E range, *the χ^2 never vanishes at any point of $|\Delta m_{31}^2(IH)|_{th}$, whichever experiment it may be derived from.* So, regardless of the precision of Δm_{atm}^2 , there will be some non-zero hierarchy sensitivity given by this χ^2 , which would obviously be scaled up with higher detector exposures and improved with better detector resolution. At the level of the survival probability, this translates to the statement that the L/E spectra of $P_{\bar{e}\bar{e}}$ for the normal and inverted hierarchies never become completely identical for any pair of possible values of $\Delta m_{31}^2(NH)$ and $\Delta m_{31}^2(IH)$.⁸ The point where they are most similar gives the minimum χ^2 .

⁷In [94], an analysis of the possibility to determine the neutrino mass hierarchy is performed using specific values of the constants c and d in eq. (4.2) ($c = \cos^2 \theta_{12}$, $d = \sin^2 \theta_{12}$), which are derived in the approximation of $\Delta m_{21}^2 L/4E \ll 1$. For the range of L/E considered by us we have $\Delta m_{21}^2 L/4E \sim 1$, and thus the indicated approximation is not valid.

⁸This observation was also made in ref. [52].

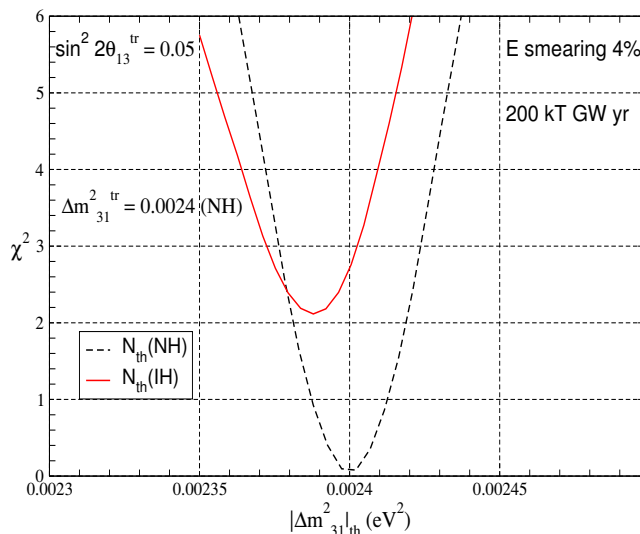


Figure 13. The function $(\chi^2)_{\text{stat}}$, marginalized over θ_{13} , versus $|\Delta m_{31}^2|$ for $\sin^2 2\theta_{13}^{\text{true}} = 0.05$ and a detector energy resolution of 4%, 200 kT GW yr detector exposure and 60 Km baseline. The figure is obtained from a 150-bin analysis in the range $L/E = 5 - 32$ Km/MeV. The true hierarchy is chosen to be normal. The dashed (solid) curve corresponds to the NH spectrum (“wrong” IH spectrum).

$(\chi^2)_{\text{stat}}^{\text{min}}$	Energy resolution		
$\sin^2 2\theta_{13}^{\text{true}}$	2%	3%	4%
0.02	0.55	0.44	0.33
0.05	3.50	2.79	2.11

Table 1. Values of $(\chi^2)_{\text{stat}}^{\text{min}}$ marginalized over the parameters θ_{13} and $|\Delta m_{31}^2|$ for two values of $\sin^2 2\theta_{13}^{\text{true}}$ and three values of the detector energy resolution, for a detector exposure of 200 kT GW yr and a baseline of 60 Km. The values are obtained in an analysis using 150 L/E bins in the range 5 - 32 Km/MeV.

4.3 Results

Table 1 lists the values of the hierarchy sensitivity $(\chi^2)_{\text{stat}}^{\text{min}}$ for different values of θ_{13} and the detector energy resolution, after a marginalization over the above parameter ranges, for an exposure of 200 kT GW yr, when a 150-bin analysis is performed. These results are with only statistical errors i.e. no systematic uncertainties) taken into account. The hierarchy sensitivity in σ is related to the 1 d.o.f. χ^2 here by the expression $\sigma = \sqrt{\chi^2}$.

Energy scale uncertainty. We have checked that including the energy scale shift and shrink/expansion in the event spectrum has no effect on the hierarchy sensitivity, either with an energy-dependent or energy-independent shrink/expansion. This is because, as observed in figures 2, 3, 11 and 12, the effect of a scale shrink/expansion and shift is identical on the event spectra for the normal and inverted hierarchies, irrespective of the

$[(\chi^2)_{\text{stat}}]_{\text{prior}}^{\text{min}}$	Energy resolution		
$\sin^2 2\theta_{13}^{\text{true}}$	2%	3%	4%
0.02	0.57	0.46	0.37
0.05	3.64	2.93	2.25

Table 2. Values of $[(\chi^2)_{\text{stat}}]_{\text{prior}}^{\text{min}}$ marginalized over the parameters θ_{13} and $|\Delta m_{31}^2|$ with priors included, for $\sin^2 2\theta_{13}^{\text{true}} = 0.02; 0.05$ and three values of the detector’s energy resolution. The baseline, detector exposure and event binning are the same as those used to obtain table 1.

different kinds of changes it produces in the spectrum for a specific hierarchy. In other words, the shift or shape variations caused by an energy scaling do not lead to any change in the relative positions and behaviour of the NH and IH spectra. Hence the hierarchy sensitivity is unaffected.

Priors. Prior experimental information regarding the other neutrino parameters can be included in the analysis in the form of ”priors”, defined as:

$$\chi_{\text{prior}}^2 = \left(\frac{|\Delta m_{\text{atm}}^2|^{\text{true}} - |\Delta m_{\text{atm}}^2|}{\sigma(|\Delta m_{\text{atm}}^2|)} \right)^2 + \left(\frac{\sin^2 2\theta_{13}^{\text{true}} - \sin^2 2\theta_{13}}{\sigma(\sin^2 2\theta_{13})} \right)^2$$

Here $|\Delta m_{\text{atm}}^2|$ and $\sin^2 2\theta_{13}$ are the values of the marginalized parameters in the N_{th} spectrum, $|\Delta m_{\text{atm}}^2|^{\text{true}}$ and $\sin^2 2\theta_{13}^{\text{true}}$ are the values fixed in the N_{ex} spectrum, and $\sigma(|\Delta m_{\text{atm}}^2|)$ and $\sigma(\sin^2 2\theta_{13})$ are the present 1σ error ranges of the respective parameters, here taken to be $\sigma(|\Delta m_{\text{atm}}^2|) = 5\% \times |\Delta m_{\text{atm}}^2|^{\text{true}}$ and $\sigma(\sin^2 2\theta_{13}) = 0.02$. This quantity serves as a penalty for moving away from the ”true” value of a parameter, since this would obviously worsen the fit with the (other) experiment(s) which measured the parameter. So adding the ”prior” term to the χ^2 and then performing the marginalization effectively minimizes the χ^2 over our data as well as that of the other experiment(s) which measured the parameters.

Table 1 lists the values of the hierarchy sensitivity $[(\chi^2)_{\text{stat}}]_{\text{prior}}^{\text{min}}$ for different values of θ_{13} and the detector energy resolution, after a marginalization over the above parameter ranges with priors taken into account, for the same values of detector exposure and event binning. There is a slight improvement in the results with the inclusion of priors. It may be noted here that if an improved 1σ error of $\sigma(|\Delta m_{\text{atm}}^2|) = 1\% \times |\Delta m_{\text{atm}}^2|^{\text{true}}$ in the atmospheric mass-squared difference is considered (which may be possible from future precision experiments), the improvement in the hierarchy sensitivity with the inclusion of the prior term is more pronounced. For example, the value of $[(\chi^2)_{\text{stat}}]_{\text{prior}}^{\text{min}}$ for $\sin^2 2\theta_{13}^{\text{true}} = 0.05$ and a detector resolution of 4% (second row, last column in table 2) becomes 2.6 in this case. Since $|\Delta m_{\text{atm}}^2|$ is likely to be determined with increasingly better precision before the hierarchy ambiguity is resolved, it may be useful to include prior information in this way from measurements of $|\Delta m_{\text{atm}}^2|$, when studying the hierarchy sensitivity of an experiment.

Detector exposure. In table 3, we give the values of the hierarchy sensitivity $[(\chi^2)_{\text{stat}}]_{\text{prior}}^{\text{min}}$ for $\sin^2 2\theta_{13}^{\text{true}} = 0.02$, for 3 different values of the detector resolution and a scaling in the detector exposure. These results show the strong dependence of the sensitivity on the

$(\chi^2)_{\text{stat}}^{\text{min}}$	$\sin^2 2\theta_{13}^{\text{true}} = 0.02$			$\sin^2 2\theta_{13}^{\text{true}} = 0.05$		
Detector exposure, kT GW yr	Energy resolution					
	2%	3%	4%	2%	3%	4%
200	0.55	0.44	0.33	3.50	2.79	2.11
400	1.10	0.88	0.66	7.0	5.58	4.22
600	1.65	1.32	0.98	10.50	8.37	6.33
800	2.20	1.75	1.30	14.0	11.15	8.40
1000	2.70	2.15	1.60	17.20	13.80	10.50

Table 3. Values of $(\chi^2)_{\text{stat}}^{\text{min}}$ marginalized over the parameters θ_{13} and $|\Delta m_{31}^2|$ for several different detector exposures (in kT GW yr), $\sin^2 2\theta_{13}^{\text{true}} = 0.02$; 0.05, three values of the detector’s energy resolution and a baseline of 60 Km, obtained in an analysis using 150 L/E bins in the range 5 - 32 Km/MeV. Including priors in the analysis increases the sensitivity to the type of the neutrino mass spectrum.

detector exposure, which is a function of the detector mass, power and time of running. In other words, the sensitivity is directly related to the statistics or total event number of the reactor experiment. Hence, a hierarchy sensitivity of $> 1.5\sigma$ may be possible even for $\sin^2 2\theta_{13}^{\text{true}} = 0.02$ with an exposure of 1000 kT GW yr and an energy resolution of 2%, and this would improve further with a higher detector mass/power. With a larger value, like $\sin^2 2\theta_{13}^{\text{true}} = 0.05$, an exposure of 1000 kT GW yr may give a hierarchy sensitivity of $> 3\sigma$ even for an energy resolution of 4%.

These results can be compared with the results for hierarchy sensitivity in [52], where the detector exposure (in kT GW yr) required to obtain a sensitivity of 1σ or 66.8% C.L., is plotted as a function of the neutrino baseline or the energy resolution of the detector. The authors of [52] find that for an energy resolution of 2%, for a baseline of 60 Km, $\sin^2 2\theta_{13} = 0.05$ and best-fit values of other parameters, an exposure of about 220-230 kT GW yr will be required to obtain a sensitivity of 1σ . Similar parameter values of the baseline, θ_{13} , detector exposure and energy resolution give $\chi_{\text{stat}}^2 = 3.5$, or a sensitivity of 1.8σ , in our analysis.

Systematic errors. Apart from the uncertainties in the neutrino parameters, the systematic uncertainties related to the detector and geo-neutrinos also need to be included in a realistic analysis. In this case, we consider 5 sources of systematic uncertainties (3 from the detector and 2 from geo-neutrinos) [52], as mentioned earlier, for which the following values are taken:

- The efficiency error, 2%.
- The uncertainty in the estimation of the detector energy resolution, 8%.
- The linear energy scale uncertainty, 1%.
- The uncertainty in the total detectable terrestrial antineutrino flux, 10%.
- The uncertainty in the ratio of $\bar{\nu}_e$ from the decay of U-238 and Th-232, 10%.

The last two errors may be quite large, but varying them to higher values has no significant effect on the results.

We take into account the above uncertainties using the method of pulls (see, e.g., [93]). In this method, the inputs (quantities having systematic uncertainties) are allowed to deviate from their standard values in the computation of $N_{th}(i)$. If the j th input deviate from its standard value by $\sigma_j \xi_j$, where σ_j is the magnitude of the corresponding uncertainty, then the value of $N_{th}(i)$ with the changed inputs is given by

$$N_{th}(i) = N_{th}(i)(std) + \sum_{j=1}^{npull} c_i^j \xi_j, \tag{4.4}$$

where $N_{th}(i)(std)$ is the theoretical rate for the i^{th} bin, calculated with the standard values of the inputs and $npull$ is the number of sources of uncertainty, which in our case is 5. The ξ_j 's are called the "pull" variables and they determine the number of σ 's by which the j th input deviates from its standard value. In eq. (4.4), c_i^j is the change in $N_{th}(i)$ when the j th input is changed by σ_j (i.e. by 1 standard deviation). The shifted event rate defines a modified χ^2 which is then minimized with respect to the pull variables.

Implementing this method with the error parameter values given above is found to have only a minimal effect on the hierarchy sensitivity. For example, the value of $[(\chi^2)_{stat}^{\min}]_{\text{prior}}$ for $\sin^2 2\theta_{13}^{\text{true}} = 0.05$ and a detector resolution of 4% (second row, last column in table 2) changes only from 2.25 to 2.26 with the inclusion of systematic uncertainties. Hence we conclude that the hierarchy sensitivity from a reactor antineutrino experiment is strongly dependent on the detector energy resolution, the exposure (statistics) and the value of the parameter θ_{13} , but has a weak dependence on the values of the systematic errors of the detector, as long as they do not exceed $\sim 10\%$, and on the flux uncertainty due to the geo-neutrinos.

5 Conclusions

In the present article we have studied the possibility to determine the type of neutrino mass spectrum, i.e., "the neutrino mass hierarchy", in a reactor $\bar{\nu}_e$ experiment with a relatively large KamLAND-like detector and an optimal baseline of 60 Km. This possibility has been previously investigated in [49], and further in [50] using the χ^2 -method, and in [51–54] using the method of Fourier transforms of simulated data and the method of maximum likelihood analysis. Here we first analyzed systematically the Fourier Sine and Cosine Transforms (FST and FCT) of simulated reactor antineutrino data with reference to their specific neutrino mass hierarchy-dependent features discussed in [53, 54]. In the second part of the study we performed a binned χ^2 analysis of the sensitivity of the simulated data to the mass hierarchy. We considered a detector with a mass of the order of 10 kT, similar to the one proposed for the Hanohano experiment [51], using a $\bar{\nu}_e$ flux from a reactor having power of 5-10 GW and thus providing high statistical samples of $\sim 10^4$ or more events. The threshold of the measured e^+ (i.e., visible) energy was set to $E_{\text{visth}} = 1 \text{ MeV}$. We have considered values of detector's energy resolution σ/E_{vis} in the interval $2\%/\sqrt{E_{\text{vis}}} - 4\%/\sqrt{E_{\text{vis}}}$; in a few cases larger values have been utilized for clarifying and illustrative purposes.

The investigation of the neutrino mass hierarchy sensitive features of the FST and FCT spectra was performed, in particular, taking into account the possibility of an energy scale uncertainty in the form of scale shrink/expansion and shift. We have considered not only energy-independent, but also energy-dependent scale factors, more specifically, scale factors which depend linearly on the energy. Our findings can be summarized as follows.

1. The hierarchy-sensitive features in both the FCT and FST spectra discussed in [53, 54] are progressively reduced in magnitude with the worsening of the detector's energy resolution (i.e., with the increasing of σ/E_{vis}).
2. An energy-independent energy scale uncertainty (shrink/expansion and shift), leaves these features substantially unchanged, since the shapes of the FST and FCT spectra suffer only sideways shifts.
3. The asymmetry feature distinguishing between the two hierarchies discussed in [53, 54] is no longer present with the inclusion of an energy-dependent energy scale shrink/expansion (compare, e.g., figure 4(a) with figure 5(b)): the absolute modulation maxima in the cases of normal hierarchical (NH) and inverted hierarchical (IH) spectra are effectively replaced by absolute modulation minima for values of the shrink factor of about 0.7% or larger, while the adjacent valleys (minima) are replaced by adjacent peaks (maxima). We have defined the quantity

$$RLP = \frac{RP - LP}{RP + LP}, \tag{5.1}$$

where RP and LP are the amplitudes of the right and left peaks adjacent to the absolute modulation minima. The asymmetry RLP has a significant positive value for the NH spectrum and a much smaller value close to zero for the IH spectrum. For smaller values of the energy-dependent shrink factor, there is a continuous left-shift and change in shape of the Fourier spectrum leading to a conversion from the RL or PV asymmetry feature to the RLP asymmetry feature. For values of the shrink factor between $\sim 0.4\% - 0.6\%$, it is difficult to identify specific asymmetry feature.

These properties of the Fourier spectra indicate that it should be possible, in principle, to extract information about the type of the spectrum the neutrino masses obey from the features present in the spectra, although the nature of the hierarchy-dependent features is changed in the case of an energy-dependent energy scale shrink/expansion.

The effect of varying the atmospheric neutrino mass-squared difference Δm_{atm}^2 over its error range, causes, in general, a change in the magnitude of the hierarchy-sensitive asymmetry features of the FST and FCT spectra without eliminating them completely.

We have performed also a statistical study of the possible sensitivity of such a reactor antineutrino experiment to the type of the neutrino mass spectrum. We adopted the method of a binned χ^2 analysis, which offers the advantages of a straightforward incorporation of i) parameter uncertainties, ii) detector characteristics like the energy resolution and energy scale uncertainty, iii) systematic errors (for which we use the method of pulls), iv) an optimized binning of data to reach the maximum possible sensitivity while being

consistent with the detector resolution, and v) the inclusion of external information on the neutrino parameters using priors. The χ^2 survey was performed using an exposure of 200 - 1000 kT GW yr, and the results were presented for different values of the detector resolution, detector exposure, and the true value of θ_{13} , with a marginalization over all neutrino parameters. The bin number was optimized at 150. The true spectrum was assumed to be with normal ordering (NH). The results of this analysis can be summarized as follows.

The hierarchy sensitivity depends strongly on the the true value of θ_{13} , the energy resolution of the detector, the detector exposure and on the binning of the spectrum data. It improves dramatically with an increase in $\theta_{13}^{\text{true}}$, increases linearly with the exposure (due to the increase in statistics), and falls significantly with worsening resolution. For example, $(\chi^2)_{\text{stat}}^{\text{min}}$ for the “wrong” hierarchy improves from 0.55 for $\sin^2 2\theta_{13}^{\text{true}} = 0.02$, an energy resolution of 2% and a detector exposure of 200 kT GW yr (corresponding to a hierarchy sensitivity of less than 1σ), to 3.5 (a sensitivity of 1.8σ) for $\sin^2 2\theta_{13}^{\text{true}} = 0.05$ for the same values of the resolution and exposure. With an exposure of 1000 kT GW yr and the same values of the resolution and $\theta_{13}^{\text{true}}$, it increases to 2.7 (1.6σ). On the other hand, if the energy resolution has a value of 3%, the $(\chi^2)_{\text{stat}}^{\text{min}}$ falls to 0.44 for the same values of $\theta_{13}^{\text{true}}$ and exposure, and a significant sensitivity ($> 2\sigma$) can be achieved only if the exposure is scaled up to higher than 1000 kT GW yr.

A marginalization over the error ranges of the parameters Δm_{atm}^2 and θ_{13} has a significant effect in the case of Δm_{atm}^2 , and a mild effect in the case of θ_{13} . Varying the solar parameters Δm_{21}^2 and θ_{12} within their 3σ ranges leaves the results essentially unchanged. Moreover, since the currently measured value of the atmospheric neutrino mass-squared difference Δm_{atm}^2 is, in general, in between Δm_{31}^2 and Δm_{32}^2 , it is important to take into account the possible range of $\Delta m_{31}^2(IH)$ and $\Delta m_{32}^2(IH)$ with respect to the assumed true values of $\Delta m_{31}^2(NH)$ and $\Delta m_{32}^2(NH)$, when computing the χ^2 sensitivity. It is found that since the $\bar{\nu}_e$ survival probability $P_{\bar{e}\bar{e}}(L/E)$ never becomes identical for any pair of possible values of $\Delta m_{31}^2(NH)$ and $\Delta m_{31}^2(IH)$ within the L/E range relevant for our analysis, the marginalized χ^2 remains non-zero over the entire allowed range of $\Delta m_{31}^2(IH)$, and, if θ_{13} is sufficiently large, it can assume significant values for the exposures and energy resolutions considered.

The sensitivity does not depend significantly on the energy scale uncertainty (up to a value of about 5%), even in the case of a scale uncertainty factor which depends linearly on the energy. This is due to the fact that the scale shift affects the event spectra in the cases of the NH and IH neutrino mass spectra in the same way. We found also that the effect of systematic errors (assumed to be smaller than $\sim 10\%$) and geo-neutrino flux uncertainties is insignificant (less than 1%).

The number of L/E bins in the analysis strongly influences the χ^2 value for the “wrong” hierarchy. The value of χ^2 increases three-fold when the bin number is increased from 40 to 150. However, the allowed bin number is constrained by the detector’s energy resolution and the requirement that the bin width is not smaller than the resolution width. Hence, the optimization of binning is important. Also, increasing the threshold of the visible energy in the analysis from $E_{\text{visth}} = 1.0 \text{ MeV}$ to $E_{\text{visth}} = 1.8 \text{ MeV}$ (i.e. putting a higher cut-off of 2.6 MeV on the $\bar{\nu}_e$ energy spectrum) significantly worsens the sensitivity, because of the

corresponding loss of statistics. If, for instance, we choose $E_{\text{visth}} = 1.8 \text{ MeV}$ and perform an analysis with 25 L/E bins, we obtain a poor $(\chi^2)_{\text{stat}}^{\text{min}} = 0.8$ even for as high a value of θ_{13} as $\sin^2 2\theta_{13}^{\text{true}} = 0.1$, an exposure of 200 kT GW yr and an energy resolution of 3%. With $E_{\text{visth}} = 1.0 \text{ MeV}$, 150 L/E bins, $\sin^2 2\theta_{13}^{\text{true}} = 0.05$ and the same values of exposure and energy resolution, we get $(\chi^2)_{\text{stat}}^{\text{min}} = 2.8$. The worsening of the hierarchy sensitivity with the increase of E_{visth} to 1.8 MeV occurs in spite of the fact that the increased threshold excludes the contribution to the signal due to geo-neutrinos. This is because the total statistics has a much more dramatic effect on the hierarchy sensitivity: in the case of a sufficiently large statistics the geo-neutrino uncertainties play essentially a negligible role.

The addition of external information in the form of priors has only a minor effect on the sensitivity ($\sim 5\%$) with the present 1σ error range of 5% in $|\Delta m_{\text{atm}}^2|$. The contribution of priors becomes important if a prospective precision of 1% on $|\Delta m_{\text{atm}}^2|$ is considered, leading to an improvement of $\sim 20\%$. For example, for a $|\Delta m_{\text{atm}}^2|$ error range of 5%, $\sin^2 2\theta_{13}^{\text{true}} = 0.05$ and a detector resolution of 4%, the value of $[(\chi^2)_{\text{stat}}^{\text{min}}]_{\text{prior}} = 2.25$ (as compared to $(\chi^2)_{\text{stat}}^{\text{min}} = 2.11$ without priors), but with an improved $|\Delta m_{\text{atm}}^2|$ error range of 1% (which may be possible from future precision experiments), the value of $[(\chi^2)_{\text{stat}}^{\text{min}}]_{\text{prior}} = 2.6$. Since the neutrino parameters are likely to be measured with improved precision before the neutrino mass hierarchy is determined, it is useful to include prior information from other experiments in this way.

Our results show that if $\sin^2 2\theta_{13}$ is sufficiently large, $\sin^2 2\theta_{13} \gtrsim 0.02$, it would be possible to get a significant information on, or even determine, the type of neutrino mass spectrum (i.e., the neutrino mass hierarchy) in a high statistics experiment with reactor $\bar{\nu}_e$ with a baseline of 60 km, using a relatively large KamLAND-like detector of mass ~ 10 kT, having an energy resolution of $\sigma/E_{\text{vis}} \sim (2\%/\sqrt{E_{\text{vis}}} - 4\%/\sqrt{E_{\text{vis}}})$ and an exposure of at least 200 kT GW yr. These requirements on the set-up are very challenging, but not impossible to realize.

Acknowledgments

We thank M. Roos for reading the manuscript and useful comments. P.G. thanks S. Uma Sankar, Danny Marfatia, Srubabati Goswami and Raj Gandhi for useful discussions and Liang Zhan for helpful communication. This work was supported in part by the INFN program on ‘‘Astroparticle Physics’’ and by the World Premier International Research Center Initiative (WPI Initiative), MEXT, Japan (S.T.P.).

References

- [1] B.T. Cleveland et al., *Measurement of the solar electron neutrino flux with the Homestake chlorine detector*, *Astrophys. J.* **496** (1998) 505 [SPIRES].
- [2] KAMIOKANDE collaboration, Y. Fukuda et al., *Solar neutrino data covering solar cycle 22*, *Phys. Rev. Lett.* **77** (1996) 1683 [SPIRES].
- [3] SAGE collaboration, J.N. Abdurashitov et al., *Measurement of the solar neutrino capture rate with gallium metal. III: Results for the 2002–2007 data-taking period*, *Phys. Rev. C* **80** (2009) 015807 [arXiv:0901.2200] [SPIRES].

- [4] GALLEX collaboration, P. Anselmann et al., *Solar neutrinos observed by GALLEX at Gran Sasso*, *Phys. Lett. B* **285** (1992) 376 [[SPIRES](#)].
- [5] GALLEX collaboration, W. Hampel et al., *GALLEX solar neutrino observations: Results for GALLEX IV*, *Phys. Lett. B* **447** (1999) 127 [[SPIRES](#)].
- [6] GNO collaboration, M. Altmann et al., *Complete results for five years of GNO solar neutrino observations*, *Phys. Lett. B* **616** (2005) 174 [[hep-ex/0504037](#)] [[SPIRES](#)].
- [7] SUPER-KAMIOKANDE collaboration, S. Fukuda et al., *Determination of Solar Neutrino Oscillation Parameters using 1496 Days of Super-Kamiokande-I Data*, *Phys. Lett. B* **539** (2002) 179 [[hep-ex/0205075](#)] [[SPIRES](#)].
- [8] SNO collaboration, Q.R. Ahmad et al., *Measurement of the charged current interactions produced by B-8 solar neutrinos at the Sudbury Neutrino Observatory*, *Phys. Rev. Lett.* **87** (2001) 071301 [[nucl-ex/0106015](#)] [[SPIRES](#)].
- [9] SNO collaboration, Q.R. Ahmad et al., *Direct evidence for neutrino flavor transformation from neutral-current interactions in the Sudbury Neutrino Observatory*, *Phys. Rev. Lett.* **89** (2002) 011301 [[nucl-ex/0204008](#)] [[SPIRES](#)].
- [10] SUPER-KAMIOKANDE collaboration, Y. Fukuda et al., *Evidence for oscillation of atmospheric neutrinos*, *Phys. Rev. Lett.* **81** (1998) 1562 [[hep-ex/9807003](#)] [[SPIRES](#)].
- [11] SUPER-KAMIOKANDE collaboration, Y. Ashie et al., *Evidence for an oscillatory signature in atmospheric neutrino oscillation*, *Phys. Rev. Lett.* **93** (2004) 101801 [[hep-ex/0404034](#)] [[SPIRES](#)].
- [12] KAMLAND collaboration, K. Eguchi et al., *First results from KamLAND: Evidence for reactor anti-neutrino disappearance*, *Phys. Rev. Lett.* **90** (2003) 021802 [[hep-ex/0212021](#)] [[SPIRES](#)].
- [13] KAMLAND collaboration, T. Araki et al., *Measurement of neutrino oscillation with KamLAND: Evidence of spectral distortion*, *Phys. Rev. Lett.* **94** (2005) 081801 [[hep-ex/0406035](#)] [[SPIRES](#)].
- [14] BOREXINO collaboration, C. Arpesella et al., *First real time detection of Be7 solar neutrinos by Borexino*, *Phys. Lett. B* **658** (2008) 101 [[arXiv:0708.2251](#)] [[SPIRES](#)].
- [15] THE BOREXINO collaboration, C. Arpesella et al., *Direct Measurement of the Be-7 Solar Neutrino Flux with 192 Days of Borexino Data*, *Phys. Rev. Lett.* **101** (2008) 091302 [[arXiv:0805.3843](#)] [[SPIRES](#)].
- [16] K2K collaboration, M.H. Ahn et al., *Measurement of Neutrino Oscillation by the K2K Experiment*, *Phys. Rev. D* **74** (2006) 072003 [[hep-ex/0606032](#)] [[SPIRES](#)].
- [17] MINOS collaboration, D.G. Michael et al., *Observation of muon neutrino disappearance with the MINOS detectors and the NuMI neutrino beam*, *Phys. Rev. Lett.* **97** (2006) 191801 [[hep-ex/0607088](#)] [[SPIRES](#)].
- [18] MINOS collaboration, P. Adamson et al., *Measurement of Neutrino Oscillations with the MINOS Detectors in the NuMI Beam*, *Phys. Rev. Lett.* **101** (2008) 131802 [[arXiv:0806.2237](#)] [[SPIRES](#)].
- [19] B. Pontecorvo, *Mesonium and anti-mesonium*, *Zh. Eksp. Teor. Fiz.* **33** (1957) 549 [*Sov. Phys. JETP* **6** (1957) 429] [[SPIRES](#)].

- [20] B. Pontecorvo, *Inverse beta processes and nonconservation of lepton charge*, *Zh. Eksp. Teor. Fiz.* **34** (1958) 247 [*Sov. Phys. JETP* **7** (1958) 172] [SPIRES].
- [21] Z. Maki, M. Nakagawa and S. Sakata, *Remarks on the unified model of elementary particles*, *Prog. Theor. Phys.* **28** (1962) 870 [SPIRES].
- [22] B. Pontecorvo, *Neutrino experiments and the question of leptonic-charge conservation*, *Sov. Phys. JETP* **26** (1968) 984 [*Zh. Eksp. Teor. Fiz.* **53** (1967) 1717] [SPIRES].
- [23] PARTICLE DATA GROUP collaboration, C. Amsler et al., *Review of particle physics*, *Phys. Lett. B* **667** (2008) 1 [SPIRES].
- [24] S.M. Bilenky and S.T. Petcov, *Massive Neutrinos and Neutrino Oscillations*, *Rev. Mod. Phys.* **59** (1987) 671 [SPIRES].
- [25] S.M. Bilenky, J. Hosek and S.T. Petcov, *On Oscillations of Neutrinos with Dirac and Majorana Masses*, *Phys. Lett. B* **94** (1980) 495 [SPIRES].
- [26] P. Langacker, S.T. Petcov, G. Steigman and S. Toshev, *On the Mikheev-Smirnov-Wolfenstein (MSW) Mechanism of Amplification of Neutrino Oscillations in Matter*, *Nucl. Phys. B* **282** (1987) 589 [SPIRES].
- [27] S.M. Bilenky, S. Pascoli and S.T. Petcov, *Majorana neutrinos, neutrino mass spectrum, CP-violation and neutrinoless double beta-decay. I: The three-neutrino mixing case*, *Phys. Rev. D* **64** (2001) 053010 [hep-ph/0102265] [SPIRES].
- [28] S.T. Petcov, *Theoretical Prospects of Neutrinoless Double Beta Decay*, *Physica Scripta T* **121** (2005) 94 [hep-ph/0504166] [SPIRES].
- [29] S. Pascoli and S.T. Petcov, *Majorana Neutrinos, Neutrino Mass Spectrum and the $| \langle m \rangle | \sim 10^{-3}$ eV Frontier in Neutrinoless Double Beta Decay*, *Phys. Rev. D* **77** (2008) 113003 [arXiv:0711.4993] [SPIRES].
- [30] S. Pascoli, S.T. Petcov and C.E. Yaguna, *Quasi-Degenerate Neutrino Mass Spectrum, $\mu \rightarrow e + \gamma$ Decay and Leptogenesis*, *Phys. Lett. B* **564** (2003) 241 [hep-ph/0301095] [SPIRES].
- [31] S.T. Petcov, T. Shindou and Y. Takanishi, *Majorana CP-violating phases, RG running of neutrino mixing parameters and charged lepton flavour violating decays*, *Nucl. Phys. B* **738** (2006) 219 [hep-ph/0508243] [SPIRES].
- [32] S.T. Petcov and T. Shindou, *Charged lepton decays $l(i) \rightarrow l(j) + \gamma$, leptogenesis CP-violating parameters and Majorana phases*, *Phys. Rev. D* **74** (2006) 073006 [hep-ph/0605151] [SPIRES].
- [33] S. Pascoli, S.T. Petcov and W. Rodejohann, *On the connection of leptogenesis with low energy CP-violation and LFV charged lepton decays*, *Phys. Rev. D* **68** (2003) 093007 [hep-ph/0302054] [SPIRES].
- [34] S.T. Petcov, W. Rodejohann, T. Shindou and Y. Takanishi, *The see-saw mechanism, neutrino Yukawa couplings, LFV decays $l(i) \rightarrow l(j) + \gamma$ and leptogenesis*, *Nucl. Phys. B* **739** (2006) 208 [hep-ph/0510404] [SPIRES].
- [35] E. Molinaro and S.T. Petcov, *A Case of Subdominant/Suppressed 'High Energy' Contribution to the Baryon Asymmetry of the Universe in Flavoured Leptogenesis*, *Phys. Lett. B* **671** (2009) 60 [arXiv:0808.3534] [SPIRES].
- [36] E. Molinaro and S.T. Petcov, *The Interplay Between the 'Low' and 'High' Energy CP-Violation in Leptogenesis*, *Eur. Phys. J. C* **61** (2009) 93 [arXiv:0803.4120] [SPIRES].

- [37] C. Hagedorn, E. Molinaro and S.T. Petcov, *Majorana Phases and Leptogenesis in See-Saw Models with A_4 Symmetry*, *JHEP* **09** (2009) 115 [[arXiv:0908.0240](#)] [[SPIRES](#)].
- [38] CHOOZ collaboration, M. Apollonio et al., *Limits on Neutrino Oscillations from the CHOOZ Experiment*, *Phys. Lett. B* **466** (1999) 415 [[hep-ex/9907037](#)] [[SPIRES](#)].
- [39] A. Bandyopadhyay, S. Choubey, S. Goswami, S.T. Petcov and D.P. Roy, *Neutrino Oscillation Parameters After High Statistics KamLAND Results*, [arXiv:0804.4857](#) [[SPIRES](#)].
- [40] G.L. Fogli et al., *Observables sensitive to absolute neutrino masses (Addendum)*, *Phys. Rev. D* **78** (2008) 033010 [[arXiv:0805.2517](#)] [[SPIRES](#)].
- [41] T. Schwetz, M.A. Tórtola and J.W.F. Valle, *Three-flavour neutrino oscillation update*, *New J. Phys.* **10** (2008) 113011 [[arXiv:0808.2016](#)] [[SPIRES](#)].
- [42] M. Mezzetto and T. Schwetz, θ_{13} : *phenomenology, present status and prospect*, *J. Phys. G* **37** (2010) 103001 [[arXiv:1003.5800](#)] [[SPIRES](#)].
- [43] N. Cabibbo, *Time Reversal Violation in Neutrino Oscillation*, *Phys. Lett. B* **72** (1978) 333 [[SPIRES](#)].
- [44] V.D. Barger, K. Whisnant and R.J.N. Phillips, *CP Violation in Three Neutrino Oscillations*, *Phys. Rev. Lett.* **45** (1980) 2084 [[SPIRES](#)].
- [45] P.I. Krastev and S.T. Petcov, *Resonance Amplification and t Violation Effects in Three Neutrino Oscillations in the Earth*, *Phys. Lett. B* **205** (1988) 84 [[SPIRES](#)].
- [46] S.T. Petcov, *Towards Complete Neutrino Mixing Matrix and CP-Violation* *Nucl. Phys. Proc. Suppl.* **143** (2005) 159 [[hep-ph/0412410](#)] [[SPIRES](#)].
- [47] ISS PHYSICS WORKING GROUP collaboration, A. Bandyopadhyay et al., *Physics at a future Neutrino Factory and super-beam facility*, *Rept. Prog. Phys.* **72** (2009) 106201 [[arXiv:0710.4947](#)] [[SPIRES](#)].
- [48] R.N. Mohapatra et al., *Theory of neutrinos: A white paper*, *Rept. Prog. Phys.* **70** (2007) 1757 [[hep-ph/0510213](#)] [[SPIRES](#)].
- [49] S.T. Petcov and M. Piai, *The LMA MSW solution of the solar neutrino problem, inverted neutrino mass hierarchy and reactor neutrino experiments*, *Phys. Lett. B* **533** (2002) 94 [[hep-ph/0112074](#)] [[SPIRES](#)].
- [50] S. Choubey, S.T. Petcov and M. Piai, *Precision neutrino oscillation physics with an intermediate baseline reactor neutrino experiment*, *Phys. Rev. D* **68** (2003) 113006 [[hep-ph/0306017](#)] [[SPIRES](#)].
- [51] J. Learned, S.T. Dye, S. Pakvasa and R.C. Svoboda, *Determination of neutrino mass hierarchy and $\theta(13)$ with a remote detector of reactor antineutrinos*, *Phys. Rev. D* **78** (2008) 071302 [[hep-ex/0612022](#)] [[SPIRES](#)].
- [52] M. Batygov et al., *Prospects of neutrino oscillation measurements in the detection of reactor antineutrinos with a medium-baseline experiment*, [arXiv:0810.2580](#) [[SPIRES](#)].
- [53] L. Zhan, Y. Wang, J. Cao and L. Wen, *Determination of the Neutrino Mass Hierarchy at an Intermediate Baseline*, *Phys. Rev. D* **78** (2008) 111103 [[arXiv:0807.3203](#)] [[SPIRES](#)].
- [54] L. Zhan, Y. Wang, J. Cao and L. Wen, *Experimental Requirements to Determine the Neutrino Mass Hierarchy Using Reactor Neutrinos*, *Phys. Rev. D* **79** (2009) 073007 [[arXiv:0901.2976](#)] [[SPIRES](#)].

- [55] S.M. Bilenky, D. Nicolo and S.T. Petcov, *Constraints on $|U(e3)|^2$ from a three-neutrino oscillation analysis of the CHOOZ data*, *Phys. Lett. B* **538** (2002) 77 [[hep-ph/0112216](#)] [[SPIRES](#)].
- [56] M. Freund, M. Lindner, S.T. Petcov and A. Romanino, *Testing matter effects in very long baseline neutrino oscillation experiments*, *Nucl. Phys. B* **578** (2000) 27 [[hep-ph/9912457](#)] [[SPIRES](#)].
- [57] A. Cervera et al., *Golden measurements at a neutrino factory*, *Nucl. Phys. B* **579** (2000) 17 [*Erratum ibid.* **593** (2001) 731] [[hep-ph/0002108](#)] [[SPIRES](#)].
- [58] V.D. Barger, S. Geer, R. Raja and K. Whisnant, *Determination of the pattern of neutrino masses at a neutrino factory*, *Phys. Lett. B* **485** (2000) 379 [[hep-ph/0004208](#)] [[SPIRES](#)].
- [59] M. Chizhov, M. Maris and S.T. Petcov, *On the oscillation length resonance in the transitions of solar and atmospheric neutrinos crossing the earth core*, [hep-ph/9810501](#) [[SPIRES](#)].
- [60] J. Bernabéu, S. Palomares Ruiz and S.T. Petcov, *Atmospheric neutrino oscillations, $\theta(13)$ and neutrino mass hierarchy*, *Nucl. Phys. B* **669** (2003) 255 [[hep-ph/0305152](#)] [[SPIRES](#)].
- [61] S. Palomares-Ruiz and S.T. Petcov, *Three-neutrino oscillations of atmospheric neutrinos, $\theta(13)$, neutrino mass hierarchy and iron magnetized detectors*, *Nucl. Phys. B* **712** (2005) 392 [[hep-ph/0406096](#)] [[SPIRES](#)].
- [62] S.T. Petcov and T. Schwetz, *Determining the neutrino mass hierarchy with atmospheric neutrinos*, *Nucl. Phys. B* **740** (2006) 1 [[hep-ph/0511277](#)] [[SPIRES](#)].
- [63] R. Gandhi, P. Ghoshal, S. Goswami, P. Mehta and S. Uma Sankar, *Earth matter effects at very long baselines and the neutrino mass hierarchy*, *Phys. Rev. D* **73** (2006) 053001 [[hep-ph/0411252](#)] [[SPIRES](#)].
- [64] R. Gandhi et al., *Mass Hierarchy Determination via future Atmospheric Neutrino Detectors*, *Phys. Rev. D* **76** (2007) 073012 [[arXiv:0707.1723](#)] [[SPIRES](#)].
- [65] S.T. Petcov, *Diffraction-Like (or Parametric-Resonance-Like?) Enhancement of the Earth (Day-Night) Effect for Solar Neutrinos Crossing the Earth Core*, *Phys. Lett. B* **434** (1998) 321 [*Erratum ibid.* **444** (1998) 584] [[hep-ph/9805262](#)] [[SPIRES](#)].
- [66] M.V. Chizhov and S.T. Petcov, *New conditions for a total neutrino conversion in a medium*, *Phys. Rev. Lett.* **83** (1999) 1096 [[hep-ph/9903399](#)] [[SPIRES](#)].
- [67] M.V. Chizhov and S.T. Petcov, *Chizhov and Petcov Reply*, *Phys. Rev. Lett.* **85** (2000) 3979 [[hep-ph/0504247](#)] [[SPIRES](#)].
- [68] M.V. Chizhov and S.T. Petcov, *Enhancing mechanisms of neutrino transitions in a medium of nonperiodic constant-density layers and in the earth*, *Phys. Rev. D* **63** (2001) 073003 [[hep-ph/9903424](#)] [[SPIRES](#)].
- [69] S. Pascoli and S.T. Petcov, *The SNO solar neutrino data, neutrinoless double-beta decay and neutrino mass spectrum*, *Phys. Lett. B* **544** (2002) 239 [[hep-ph/0205022](#)] [[SPIRES](#)].
- [70] S. Pascoli and S.T. Petcov, *Addendum: The SNO Solar Neutrino Data, Neutrinoless Double Beta-Decay and Neutrino Mass Spectrum*, *Phys. Lett. B* **580** (2004) 280 [[hep-ph/0310003](#)] [[SPIRES](#)].
- [71] S.M. Bilenky, M.D. Mateev and S.T. Petcov, *A comment on the measurement of neutrino masses in beta-decay experiments*, *Phys. Lett. B* **639** (2006) 312 [[hep-ph/0603178](#)] [[SPIRES](#)].

- [72] K. Eitel et al., *Direct neutrino mass experiments*, *Nucl. Phys. Proc. Suppl.* **143** (2005) 197.
- [73] P. Vogel and J. Engel, *Neutrino Electromagnetic Form-Factors*, *Phys. Rev. D* **39** (1989) 3378 [SPIRES].
- [74] P. Vogel and J.F. Beacom, *The angular distribution of the neutron inverse beta decay, $\bar{\nu}_e + p \rightarrow e^+ + n$* , *Phys. Rev. D* **60** (1999) 053003 [hep-ph/9903554] [SPIRES].
- [75] T2K collaboration, Y. Hayato, *T2K at J-PARC*, *Nucl. Phys. Proc. Suppl.* **143** (2005) 269 [SPIRES].
- [76] P. Huber, M. Lindner, M. Rolinec, T. Schwetz and W. Winter, *Prospects of accelerator and reactor neutrino oscillation experiments for the coming ten years*, *Phys. Rev. D* **70** (2004) 073014 [hep-ph/0403068] [SPIRES].
- [77] P. Huber, M. Lindner, M. Rolinec, T. Schwetz and W. Winter, *Combined potential of future long-baseline and reactor experiments*, *Nucl. Phys. Proc. Suppl.* **145** (2005) 190 [hep-ph/0412133] [SPIRES].
- [78] <http://lbne.fnal.gov/>.
- [79] DOUBLE CHOOZ collaboration, F. Ardellier et al., *Double CHOOZ: A search for the neutrino mixing angle $\theta(13)$* , [hep-ex/0606025](https://arxiv.org/abs/hep-ex/0606025) [SPIRES].
- [80] DAYA-BAY collaboration, X. Guo et al., *A precision measurement of the neutrino mixing angle $\theta(13)$ using reactor antineutrinos at Daya Bay*, [hep-ex/0701029](https://arxiv.org/abs/hep-ex/0701029) [SPIRES].
- [81] Daya Bay homepage <http://dayawane.ihep.ac.cn/>.
- [82] RENO collaboration, J.K. Ahn et al., *RENO: An Experiment for Neutrino Oscillation Parameter θ_{13} Using Reactor Neutrinos at Yonggwang*, [arXiv:1003.1391](https://arxiv.org/abs/1003.1391) [SPIRES].
- [83] S. Choubey and S.T. Petcov, *Reactor anti-neutrino oscillations and gadolinium loaded Super-Kamiokande detector*, *Phys. Lett. B* **594** (2004) 333 [hep-ph/0404103] [SPIRES].
- [84] J.F. Beacom and M.R. Vagins, *GADZOOKS! Antineutrino spectroscopy with large water Cherenkov detectors*, *Phys. Rev. Lett.* **93** (2004) 171101 [hep-ph/0309300] [SPIRES].
- [85] A. Bandyopadhyay, S. Choubey and S. Goswami, *Exploring the sensitivity of current and future experiments to $\Theta(\text{odot})$* , *Phys. Rev. D* **67** (2003) 113011 [hep-ph/0302243] [SPIRES].
- [86] A. Bandyopadhyay, S. Choubey, S. Goswami and S.T. Petcov, *High precision measurements of $\Theta(\text{solar})$ in solar and reactor neutrino experiments*, *Phys. Rev. D* **72** (2005) 033013 [hep-ph/0410283] [SPIRES].
- [87] H. Minakata, H. Nunokawa, W.J.C. Teves and R. Zukanovich Funchal, *Reactor Measurement of θ_{12} : Principles, Accuracies and Physics Potentials*, *Phys. Rev. D* **71** (2005) 013005 [hep-ph/0407326] [SPIRES].
- [88] A. Donini, E. Fernandez-Martinez, D. Meloni and S. Rigolin, *ν_μ disappearance at the SPL, T2K-I, NO ν A and the neutrino factory*, *Nucl. Phys. B* **743** (2006) 41 [hep-ph/0512038] [SPIRES].
- [89] K. Anderson et al., *White paper report on using nuclear reactors to search for a value of θ_{13}* , [hep-ex/0402041](https://arxiv.org/abs/hep-ex/0402041) [SPIRES].
- [90] NO ν A collaboration, D.S. Ayres et al., *NO ν A proposal to build a 30-kiloton off-axis detector to study neutrino oscillations in the Fermilab NuMI beamline*, [hep-ex/0503053](https://arxiv.org/abs/hep-ex/0503053) [SPIRES].

- [91] S.T. Dye et al., *Earth Radioactivity Measurements with a Deep Ocean Anti-neutrino Observatory*, *Earth Moon Planets* **99** (2006) 241 [[hep-ex/0609041](#)] [[SPIRES](#)].
- [92] M.V. Diwan et al., *Very long baseline neutrino oscillation experiments for precise measurements of mixing parameters and CP-violating effects*, *Phys. Rev. D* **68** (2003) 012002 [[hep-ph/0303081](#)] [[SPIRES](#)].
- [93] G.L. Fogli, E. Lisi, A. Marrone, D. Montanino and A. Palazzo, *Getting the most from the statistical analysis of solar neutrino oscillations*, *Phys. Rev. D* **66** (2002) 053010 [[hep-ph/0206162](#)] [[SPIRES](#)].
- [94] H. Minakata, H. Nunokawa, S.J. Parke and R. Zukanovich Funchal, *Determination of the neutrino mass hierarchy via the phase of the disappearance oscillation probability with a monochromatic anti-electron-neutrino source*, *Phys. Rev. D* **76** (2007) 053004 [*Erratum* *ibid.* **D 76** (2007) 079901] [[hep-ph/0701151](#)] [[SPIRES](#)].